Lawrence Berkeley National Laboratory
Recent Work

Title

Work Hardening Behavior in Aluminum Alloy 2090

Permalink

https://escholarship.org/uc/item/2jg5p0d0

Author
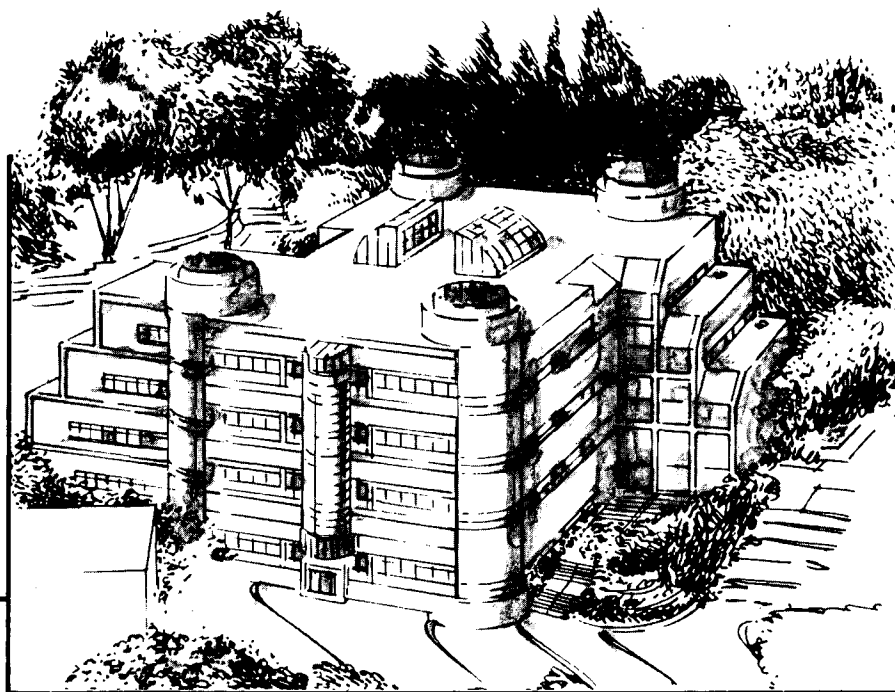
Tseng, C.

Publication Date

1993-12-01

Center for Advanced Materials

CAM

Work Hardening Behavior in Aluminum Alloy 2090

C. Tseng
(M.S. Thesis)

December 1993

Materials and Chemical Sciences Division

Lawrence Berkeley Laboratory • University of California

ONE CYCLOTRON ROAD, BERKELEY, CA 94720 • (415) 486-4755

DISCLAIMER

Work Hardening Behavior in Aluminum Alloy 2090

Carol Tseng

Master of Science Thesis

Center for Advanced Materials
Materials Sciences Division
Lawrence Berkeley Laboratory
University of California

and

Department of Materials Science and Mineral Engineering
University of California at Berkeley
Berkeley, California 94720

December 1993

Work Hardening Behavior in Aluminum Alloy 2090

Carol Tseng

ABSTRACT

An investigation into the work hardening behavior of an aluminum alloy 2090-T81 (Vintage III composition of Al-3.05Cu-2.16Li-0.12Zr in wt. %) at various test temperatures, heat treatment conditions and microstructures was conducted. One microstructure consisted of unrecrystallized, highly textured grains, and the other microstructure was composed of recrystallized grains. Microstructural effects on work hardening were divided into two levels of contribution: the grain structure level, which consisted of the grain size and shape, subgrains and texture, and the microconstituent level, which included the precipitates and solutes. Two heat treatments were studied: the as-received, peak-aged condition, and the solution heat treated condition where the as-received plate was resolutionized. Observations of the deformed surface of both as-received grain structures at various prestrains indicated that there was no correlation between an increase in slip homogeneity and an increase in work hardening. The increase in out-of-plane grain rotation at lower temperatures was not primarily responsible for the increase in work hardening. In addition, the fully plastic deformation microstructure for the unrecrystallized microstructure appeared very inhomogeneous as the grains deformed in bands; there were also bands of grains that had very little to no deformation. From the work hardening plots it was found that an unrecrystallized, {110}<112> textured grain structure with a homogeneous distribution of subgrains produced the highest rate of work hardening between 300 K and 77 K. When the microconstituents are added to both grain structures, both the work hardening rate in the elastic-plastic and fully plastic regimes and the level of work hardening at which the elastic-plastic to fully plastic transition occurred were affected. As a consequence, the elastic-plastic region may be important to the subsequent work hardening behavior in this alloy. Finally, removal of the microconstituents aided both microstructures in attaining well developed, fully plastic states at 300 K and 200 K.

LIST OF FIGURES

LIST OF TABLES

ACKNOWLEDGEMENTS

1. INTRODUCTION

Ever since the introduction of 2090-T81, numerous researchers have tried to characterize the work hardening behavior of this alloy[1-3]. In the first production of this material (Al-2.7Cu-2.2Li-0.1Zr in wt.%), Vintage I, the increase in work hardening with decreasing temperature was thought to have been attributed to the highly elongated, highly textured grain structure[1]. Additional observations of the surface deformation characteristics showed that there was an increase in out-of-plane grain rotation when the test temperature decreased from 300 K to 77 K[1,2]. It was believed that this increase in out-of-plane grain rotation resulted from the difficulty of slip transmission from grain to grain at lower temperatures, consequently, the work hardening increased. Jata and Starke[4] had found earlier in this alloy that an increase in slip homogeneity, described an increase in slip band width and a decrease in spacing between bands, caused a simultaneous increase in fracture toughness and strain hardening exponent. Yao, et al.[2] surmised that the increase in out-of-plane rotation of grains promoted greater slip homogeneity. Therefore, the work hardening increased.

Work on the next production of 2090 (Al-3.05Cu-2.16Li-0.12Zr in wt. %), Vintage III, revealed that microstructure played an important role in work hardening[3]. The 12.7 mm (0.5 in) plate used in the study was composed of two different microstructures: an unrecrystallized microstructure with a {110}<112> texture near the center of the plate and a recrystallized microstructure with an undetermined texture on each side of the unrecrystallized microstructure; the location of these microstructures in the plate is shown in figure 1. These microstructures behaved very differently as the test temperature decreased from 300 K to 4 K with the unrecrystallized microstructure showing a much higher increase in work hardening. Since both microstructures originated from the same plate, they had the same nominal composition and had undergone the same nominal thermomechanical process. Any differences in work hardening were thus due to differences in microstructure arising from local variations in the thermomechanical processing. The most obvious microstructural difference was the grain structures.

1.1 Background of 2090

Commercial interest in 2090 arose in the hopes of creating a lighter, yet stiffer and stronger alternative to aluminum alloy 7075-T6 for use in the aircraft industry[1]. Preliminary investigations of the mechanical properties of this material discovered that this alloy also had excellent cryogenic properties; both the strength and toughness increased with decreasing temperature[5-10]. Despite these improvements in the mechanical properties, in-plane and through thickness yield strength anisotropies continued to plague this material due to its highly elongated and highly textured grain structure, even though Vintage III 2090 was processed with the intention of reducing the anisotropies found in Vintage I.

1

1.1.1 Physical Metallurgy of 2090

The Vintage III plate undergoes a proprietary thermomechanical reduction process, and the final heat treatment consists of a solution heat treatment at 550°C, a quench, a 6-8% stretch, and an aging for peak strength at 163°C for 24 hours. The unrecrystallized microstructure has a {110}<112> texture. Both microstructures consist of highly elongated grains. There are several second phases in the material[1,12], and the pertinent ones are listed in Table 1.

2090 primarily relies upon precipitation hardening for its strength. The primary strengthening phases are $\delta'(Al_3Li)$ and $T_1(Al_2CuLi)$; their characteristics are listed in Table 1. δ' is a spherical, coherent precipitate with an ordered $L1_2$ structure. δ' provides order strengthening. The first dislocation to encounter the precipitate will shear through and set up an antiphase boundary. This resulting higher energy state impedes the motion of the next dislocation passing through[11,12]. When a second dislocation passes through the same plane, order is restored. Thus, superdislocation pairs form. Although the antiphase boundary aids in strengthening the material, the reduction in the precipitate diameter after the passage of a superdislocation pair contributes to work softening. Slip along this plane becomes easier, and this deformation mode results in planar slip. The localization of slip contributes to the heterogeneity of slip.

The heterogeneity of slip decreases with the introduction of T_1. Homogenization of slip can be achieved with T_1 in a number of ways. T_1 is a semi-coherent, plate-like precipitate; its habit plane is on the {111} planes. The misfit strain between T_1 and the matrix offers some hardening[12,13]. There is also the inverse relationship between T_1 and δ'. An increase in volume fraction of T_1 reduces the volume fraction of δ'[13,14]. A reduction in the δ' population subsequently reduces the amount of planar slip. When dislocations encounter T_1, they generally bypass or tangle with it, although some shearing has been observed[15,16].

Table 1- Important second phases in 2090-T81.

Phase	Composition	Crystal Structure	Morphology	Habit Plane
δ'	Al_3Li	$L1_2$	Spherical	
T_1	Al_2CuLi	Hexagonal	Plate	{111}
β'	Al_3Zr	$L1_2$	Spherical	

Because T_1 nucleates heterogeneously, it is difficult to obtain a homogeneous distribution throughout the material. To ensure a homogeneous distribution, the plate material is stretched during the final heat treat. This stretch provides dislocations and dislocation tangles on the {111} planes and upon aging, T_1 will nucleate at these sites. Lee and Kim[17] have found, however, that the four T_1 variants are not equally distributed on the {111} planes. The "inclined" planes (1$\bar{1}$1) and ($\bar{1}$11) are heavily populated while the "edge-on" planes (111) and (11$\bar{1}$) are somewhat populated.

1.1.2 Microstructural Effects on Work Hardening

In light of the presence of the various microstructural features in 2090, it is difficult to prove that the grain structure is the only feature responsible for the differences in the work hardening temperature dependencies between the unrecrystallized and recrystallized microstructures. There are many factors that can contribute to the work hardening behavior of this material: grain size and shape, subgrains, texture, precipitates and solutes. Many researchers have attempted to define the role of each of these to work hardening in less complex materials. Their findings and a general introduction to work hardening theory are treated below.

1.2 Background on Work Hardening

In general, work hardening reflects the balance between hardening and recovery, or softening. The work hardening rate increases when hardening processes dominate. During hardening, dislocation motion is impeded by tangles, and more than one slip system is active; the mean free path of the dislocations is dictated by dislocation-dislocation interactions. Competing against hardening are recovery processes. Recovery, or work softening, involves thermally or mechanically activated softening processes such as cross slip, dislocation rearrangement, and dislocation annihilation. Recovery usually overtakes hardening contributions, thus decreasing the work hardening rate. At small strains, many materials may undergo a period of pure hardening, often referred to as Stage II work hardening. With higher strains recovery processes gain increasing importance as dislocation barriers break down. Since aluminum has a low melting point and a high stacking fault energy, this pure hardening region is not observed at room temperature. Room temperature is approximately one-third of the melting temperature, and consequently, work softening processes readily occur. In addition, the high stacking fault energy facilitates cross slip. With the presence of precipitates, it is expected that the work hardening in 2090-T81 will begin with recovery overtaking hardening processes since the dislocation mean free path now depends on precipitate spacing.

Temperature also alters the work hardening curve. As temperature is lowered, thermally activated processes such as cross slip become increasingly difficult. Dislocation mobility also decreases with decreasing temperature; thus, work hardening will increase. Kocks has found that as temperature decreases, the slope of the fully plastic region becomes less negative[18]; this region will be defined below. The initial work hardening rate is independent of temperature, but as the deformation increases, the work hardening becomes dependent on temperature.

Work hardening is also closely related to the degree of slip homogeneity during deformation. As discussed above, slip is homogeneous when the spacing between slip

planes is small and the width of the slip bands is wide[4]. Deformation, then is distributed over a wider area of the matrix, and the work hardening rate increases. If, for the same material, the slip spacing is large and the slip band width narrow, then the same amount of deformation is being confined to fewer slip planes and contributes to the localization of deformation. This deformation mode is considered heterogeneous slip and adds to the work softening process.

1.2.1 Work Hardening and Microstructure

There have been myriad theories relating work hardening and microstructure. Most of the investigations have concentrated on the effect of grain structure[18-23], and solutes[24]. To some extent, precipitates[12,26] have been studied. The effects of subgrains and texture are not well understood. All of these works have been devoted to simpler systems where the effect of one, or at most two, features on work hardening is investigated. Perhaps the most thorough treatment on work hardening is the Kocks-Mecking model. The results of these studies of grain structure, solutes and precipitates will be covered below.

One of the first to propose a model for polycrystalline materials was Taylor[20]. He related single crystal deformation behavior to polycrystalline behavior by assuming that all grains in the aggregate experienced the same strain. His model assumed that the work hardening was independent of grain size and that deformation was homogeneous. Later researchers concluded that his model fairly accurately described the behavior of polycrystalline materials with large grain sizes at large strains.

The first significant contribution to understanding the effect of grain boundaries on work hardening was conducted by Ashby[21]. He introduced the concept of the generation of two types of dislocations during deformation: statistically stored dislocations and geometrically necessary dislocations. During deformation, statistically stored dislocations were generated and tangled with each other. But, if each grain was allowed to deform independently, the grains would not fit back together again; voids and regions of overlap would occur. To maintain material continuity, geometrically necessary dislocations were needed. The non-uniform strain in the material produced these geometric dislocations, especially near grain boundaries.

In alloyed polycrystals the addition of a solute usually lowers the stacking fault energy. Dislocations now dissociate more easily, and the width between the partials increases. Cross slip becomes more difficult, thus the work hardening rate increases[27]. The addition of a solute can produce varied work hardening behaviors that are difficult to classify[24,25]. There have been many models proposed by various researchers linking solution hardening and work hardening, most of which are concerned with the superposition of solute effects with other mechanical behavior aspects[24]. One model utilizes the principle of superposition[24,25]. It assumes that solute atoms add a friction stress τ_f to all other contributions, τ_d, to constitute the total glide resistance stress τ:

$$\tau = \tau_f(c) + \tau_d(\rho).$$

4

τ_d is the stress due to dislocation-dislocation interactions and depends on the dislocation density ρ; τ_f depends on the solute concentration c. This equation describes an upward shift in the stress-strain curve as the solute concentration increases. This upward shift is not commonly observed.

Some materials, upon solute addition, have stress-strain curves that diverge from the pure material with increasing strain. This divergence is accounted for in the multiplicative hardening model, which hypothesizes that the solute hardening and the work hardening are proportional to each other. The equation is given as

$$\tau = \tau_f(c) + \left(1 + k(c)\right)\tau_d(\rho),$$

where k(c) is the proportionality constant, and it represents the interaction between solution hardening and strain hardening. This equation also accounts for the effects of the friction stress as well as the dislocation-dislocation interaction stress. Al-Mg systems display such behavior.

The relationship between precipitates and work hardening depends on whether the precipitates contribute to homogeneous slip or heterogeneous slip. Spherical coherent precipitates are usually sheared as described above for δ'. The initial strengthening offered by the precipitate is counteracted with softening after the first superdislocation pair passes through. The ease with which ensuing superdislocation pairs pass through, on the same slip plane, decreases the work hardening. The confining of slip to just a few planes localizes the deformation and leads to heterogeneous slip, further decreasing work hardening. On the other hand, semi-coherent precipitates, such as T_1, act in two ways to increase work hardening. First, the interfacial energy between the precipitate and matrix at the semi-coherent interface can act as a dislocation source[12,27]. Second, when dislocations encounter these precipitates, they bypass, rather than shear the precipitate. Bypassing increases homogeneous slip, thereby increasing work hardening.

1.2.2 The Kocks-Mecking Model

The most widely accepted model for work hardening is the Kocks-Mecking (KM) model[18,19,28,29]. Their model, schematically diagrammed in figure 2, proposes that when the work hardening rate θ is plotted versus the true stress σ, there is a linear regime after a break in the curve that is termed the fully plastic regime. This linear regime is the central part of work hardening theory and can be described by the equation

$$\theta = \theta_0 - k_2\sigma \qquad (1)$$

where θ_0 is an athermal constant that reflects the dislocation storage rate and $k_2\sigma$ is the dynamic recovery term; the derivation of this equation is given in Appendix A. For a particular, well annealed material, there is a characteristic θ_0 value, regardless of the grain structure; grain structure here describes grain size and shape. The dynamic recovery term

describes work softening processes by which dislocations will rearrange and/or annihilate. The fully plastic state as described here is a theoretical construction; the appearance of the deformation microstructure is not well defined. Notice that the region dropping down from the modulus value to the fully plastic region is not regarded to have any impact on the work hardening. Microstructure affects this portion of the curve, but after the transition into the fully plastic state, the dislocation density is so high that dislocation-dislocation interactions dominate the work hardening behavior. The KM model does describe the behavior of pure, FCC materials quite well.

1.2.3 Significant Features of the Work Hardening Curve

To evaluate the effect of microstructural features on work hardening there are several aspects of the work hardening curve on which to focus. The work hardening rate (θ) can be plotted versus either true strain (ε) or true stress (σ) (figure 3). Since strain is dependent on the deformation history of the specimen, it is not a state variable. The θ vs. ε plots are useful in determining whether the test specimen has fulfilled the necking criterion, where $\theta = \sigma$, and the amount of uniform elongation attained. True stress, on the other hand, is a thermodynamic variable and is therefore not dependent upon the deformation path. It is more useful, then, to plot θ versus σ. This plot can be divided into two basic regions: the elastic-to-plastic transition region and the fully plastic, or bulk plasticity, region. The former is the steep drop from the elastic modulus. Those grains that have more favorable crystallographic orientations will deform first. This region is believed to be influenced by microstructural features such as grain size and shape, precipitates, solutes, initial dislocation density, subgrains and texture. After the break in the work hardening curve, the approximately linear region is considered the fully plastic region, as described by the KM model. In this region, either all grains have deformed or those grains that have deformed at the end of the elastic-plastic transition region continue to do so while those that have not deformed will not. The high amount of deformation in this region results in a high dislocation density. Due to the high dislocation density, a dislocation is more likely to encounter another dislocation than a precipitate or a grain or subgrain boundary. Thus, dislocation-dislocation interactions have been generally considered the controlling feature in work hardening in the fully plastic regime. Although the fully plastic state has been discussed in theory[18,19], how the deformation microstructure should appear is generally unknown.

Since the mechanical properties and work hardening behavior of 2090 have been evaluated from tensile tests, the duration of the work hardening curve is limited by the necking criterion $\theta = \sigma$. Many researchers perform tests in torsion in order to avoid such a constraint[18,19]. Work hardening has then been observed to reach near zero values where, on the stress-strain curve, the stress tends to approach a saturation value. Tensile tests, however, provide important design criterion information such as yield strength and uniform elongation.

The ideal work hardening curve, as depicted in figure 4, would have zero slope in the fully plastic state[30]. In this ideal case, work softening does not occur, and, from equation (1), the work hardening maintains a constant value at θ_0. The material is then

experiencing pure hardening. For those materials that do not experience pure hardening, such as 2090, the ideal work hardening curve should have a work hardening rate that is slightly higher than the necking criterion, as shown in figure 5. The work hardening rate would be very low initially and then increase with increasing stress. This behavior is rarely observed.

Based on the ideal curve in figure 5, there are three significant features of the work hardening curve to consider. The first is the slope of the fully plastic region; the less negative the slope the better (figure 6a). Second is the value of the work hardening rate (figure 6b). Third is the location of the transition from elastic-plastic to fully plastic occurs (figure 6c).

1.3 Objective

Due to the difficulty in experimentally isolating the effect of one microstructural feature on work hardening in a complex commercial alloy, the objective of this work is to assess the relative contributions of grain structure, which includes the grain size and shape, subgrains and texture, and of the microconstituents, which include precipitate structure and solutes, to the work hardening between 300 K and 77 K. Any differences in dislocation structure should have been annealed out during the peak aging treatment. T_1 precipitation during this treatment should occur at dislocation tangles and on dislocations, and any remaining dislocation structures that T_1 did not nucleate on should have annealed out during the aging process. The influences of the two microstructural levels can be separated by a solution heat treatment before tensile testing. The solution heat treatment will dissolve the precipitates, and upon quenching, only δ' will precipitate out; the treatment will not alter the grain structure. The influence of grain structure and microconstituents on the work hardening curve features serves as a first step in understanding the relationship between microstructure and work hardening. Additional information about how a particular microstructural feature alters the work hardening can be provided by testing at several temperatures, especially those temperatures that simulate service conditions. Ultimately, an ideal microstructure can be defined and processed to furnish the best work hardening behavior.

2. EXPERIMENTAL PROCEDURE

The Vintage III 2090-T81 alloy used in this study was supplied by ALCOA in the form of a 12.7 mm (0.5 in) thick plate. The -T81 condition referred to a post reduction heat treatment consisting of a solution heat treatment, a quench, a stretch and a peak aging. The nominal composition of this plate is given in Table 2.

As-received (AR) specimens were examined by optical microscopy and transmission electron microscopy (TEM). Optical specimens were mechanically ground down to 600 grit on silicon carbide paper, polished down to 0.05 μm, and then etched with Keller's Reagent (2.5% HNO_3, 1.5% HCl, 0.5% HF). TEM specimens from the L-plane were prepared by cutting a 0.38 thick mm (0.015 in) slice, mechanically polishing the slice to a thickness of 0.15-0.20 mm (0.006-0.008 in), punching a 3 mm disk, and then electropolishing by the double jet technique. The electropolishing conditions were -30°C at 18-20 volts in a 1:3 solution of nitric acid and methanol.

Table 2- Composition of 2090 in weight percent[3].

Element	Composition Range	Vintage III 2090-T81
Al	bal	bal
Cu	2.4-3.0	3.05
Li	1.9-2.6	2.16
Zr	0.08-0.15	0.12
Fe	0.12	0.08
Others	< 0.05	< 0.01

Longitudinal tensile specimens of each microstructure were obtained from the plate by first using a diamond wafering blade to cut between the adjacent microstructures (see figure 1). The same plate was utilized instead of processing a plate of uniform microstructure for each microstructure. The presence of β' in the plate inhibits recrystallization, therefore, recreating the recrystallized microstructure is extremely difficult. The unrecrystallized microstructure specimens were milled down to eliminate the recrystallized microstructure and were variable in thickness, and the recrystallized microstructure specimens were approximately 2.54 mm (0.1 in) thick. The specimens were then machined to the dimensions depicted in figure 7. Specimens for slip line analysis and surface relief observations were polished down to 0.05 μm, while specimens for mechanical properties and work hardening characteristics were ground down on all four sides to 600 grit on silicon carbide paper. Tensile tests for the as received specimens were done at 300 K, 200 K, 77 K and 4 K. Specimens for surface relief and slip line analysis were strained to plastic strain values of either 0.5%, 1.5%, 2.75%, and 3.5% for a particular test temperature, although not all strains were done at all temperatures; the test matrix is listed in Table 3.

Table 3- Tensile test matrix.

Microstructure/ Heat treatment condition	300 K	200 K	77 K	4 K
Unrecrystallized (AR)	X	X	X	X
Recrystallized (AR)	X	X	X	X
Unrecrystallized (SHT)	X	X	X	
Recrystallized (SHT)	X	X	X	

The tensile data were gathered by a computer, compressed, converted to engineering stress and engineering strain, and then converted to true stress and true strain. Work hardening curves were obtained by taking the true stress-strain data, smoothing the data with a cubic spline fit, and finally taking the derivative of the fitted curve.

Surface relief observations were made with an optical microscope. Both an optical microscope and a scanning electron microscope (SEM) were used to photograph slip bands for slip band analysis. Slip band analysis was performed by the line-intercept method on all strained specimens; at least 1,000 bands were counted over many grain orientations for each specimen. Although it is customary to calculate the average slip band spacing for slip bands having the same orientation, by taking at least 1,000 slip band counts over many orientations, the orientational effect on the slip band analysis should be averaged out. Surface slip band analysis offered a way to quantify slip homogeneity between the two AR microstructures.

Surface profilometry was used on both microstructures to quantify the relative amount of surface roughness, or out-of-plane grain rotation due to deformation, for each microstructure. Surfaces were profiled for specimens strained to 3.1%±0.3% at 300 K and 77 K. A profilometer connected to a computer was used. The data were gathered by a computer, and then the average slope was subtracted from the data to eliminate any effects due to tilting of the specimen. Roughness average (R_a) values were computed by applying the formula

$$R_a = \frac{\int_0^L y(x)dx}{L}$$

where
y(x) = surface height from the average surface height value,
x = distance traveled from the origin,
L = the total distance measured.

To pattern the deformation of the fully plastic state of the unrecrystallized microstructure, the 3%, 77 K tensile specimen was mapped through the thickness. The deformation pattern was sketched based upon observations through the optical microscope.

Solution heat treated (SHT) samples were first machined to the dimensions in figure 7, heated in a circulating air furnace at 550°C for 45 minutes and then quenched in ice water; this heat treatment does not alter the grain structure. The precipitates will resolutionize, and upon quenching, δ' will precipitate out. The size of δ' will be smaller, and δ' will be more numerous than in the AR condition. The precipitate structure and solute content should be the same in both grain structures because only β' and δ' will remain after solution heat treatment, and both are spherical precipitates that nucleate homogeneously. TEM was performed to verify that T_1 was not present in the microstructure and that only β' and δ' remained. The tensile specimens were then ground on all four sides down to 600 grit. Tensile tests were performed at 300 K, 200 K, and 77 K.

3. RESULTS

3.1 Microscopy

3.1.1 As-Received Specimens

Optical micrographs of the grain structures are shown in figure 8. Near the middle of the plate, the unrecrystallized grain structure appears to be very thin in the short direction with pancake shaped grains in the rolling plane (S plane). The grain size of the pancake shaped grains is approximately 5500 x 400 x 40 μm. This unrecrystallized microstructure is surrounded on both sides by the recrystallized grain structure. The dimensions of these grains is approximately 18,000 x 850 x 150 μm.

TEM reveals further differences between the two microstructures. In figure 9 both micrographs are taken from the same area and show that the unrecrystallized microstructure has extensive subgrain formation throughout the grains. The subgrain size is approximately 2-10 μm in this plane. Figure 9a shows several grains with subgrains distributed throughout them, and figure 9b shows one grain with a homogeneous distribution of subgrains. The recrystallized microstructure, however, does not display such extensive subgrain formation throughout the grains. In figure 10a there are two very large grains with several small grains located between them. No subgrains are seen in this micrograph. Some subgrain formation is observed in figure 10b. Again, several small grains appear between very large grains, and there is some subgrain formation.

An additional difference between the two microstructures is the texture. The unrecrystallized grains have a strong tendency to be oriented in the 112 pole, as expected from the plane from which it was cut. With the recrystallized grains, however, the texture is not as obvious. Some of the grains show a tendency towards the 110 pole. These results are consistent with previous work[3] where the mechanical property data and optical microscopy observations indicate that the grain structure near the middle of the plate is composed of unrecrystallized, highly textured grains while the quarter thickness regions have undergone a recrystallization during the reduction process and before the final heat treatment.

3.1.2 Solution Heat Treated

No evidence for T_1 precipitation can be seen under TEM (figure 11). δ' is present but difficult to resolve; the mottled appearance of the grain interiors is due to δ'. Miyasato has found that the size of δ' after a solution heat treat and an ice water quench is around 6 nm[12]. The large spherical particles in the micrograph are a δ'/β' composite[12]. Under diffraction conditions, δ' spots are visible while no T_1 streaks are seen.

3.2 Mechanical Properties

3.2.1 As-Received

The mechanical properties of each microstructure at the various test temperatures are listed in Table 4. Note that there is a monotonic increase in the yield and tensile strengths for both microstructures as the temperature decreases. There is a much smaller increase between 300 K and 200 K than between the other test temperatures. The uniform and total elongations, however, have their lowest values at 200 K. The unrecrystallized microstructure has higher yield and ultimate tensile strengths at all temperatures. The elongations for the unrecrystallized microstructure are consistently lower than the recrystallized microstructure values by 21-40% from 77 K to 300 K. Little evidence of necking is observed in all specimens, but the necking criterion is satisfied in all cases.

3.2.2 Solution Heat Treated

Solution heat treating the specimens dramatically changes the mechanical properties. From Table 5 it can be seen that the strengths drop by 70-77% from the AR values. The elongations, on the other hand, increase by as much as 250-345%. The dip in elongation at 200 K in the AR condition mentioned above is also apparent in the SHT unrecrystallized case, but not as pronounced. In addition, the yield and ultimate tensile strengths for the unrecrystallized microstructure at 200 K slightly decrease from the 300 K strengths.

Table 4- Mechanical properties for the AR tensile specimens at various test temperatures.

	Yield Strength [MPa]	Ultimate Strength [MPa]	Uniform Elongation [%]†	Total Elongation [%]†
Unrecrystallized				
300	479	515	4.4	5.5
200	548	586	2.8	3.0
77	578	671	6.7	7.0
4	617	746	7.2*	7.9*
Recrystallized				
300	411	454	7.5	10.0
200	431	477	4.8	5.8
77	458	504	8.5	9.3
4	509	565	10.0	11.0

*Specimen fractured at pin.
†Based on a 1 in. gauge length.

Table 5- Mechanical properties of SHT specimens at various test temperatures.

	Yield Strength [MPa]	Ultimate Strength [MPa]	Uniform Elongation [%]†	Total Elongation [%]†
Unrecrystallized				
300	146	307	16.3	18.1
200	133	274	15.7	19.3
77	165	406	24.1	26.6
Recrystallized				
300	95	248	33.2	37.0
200	119	218	35.2	39.4
77	123	290	49.5*	49.5*

*Highest strain attainable with extensometer.
†Based on a 1 in. gauge length.

3.3 Work Hardening Behavior

3.3.1 As-Received

A look at their work hardening curves in figure 12 reveals that the two microstructures behave very differently; their work hardening rates (θ) are plotted versus true stress (σ). The most noticeable difference is their temperature dependencies. The unrecrystallized microstructure has a dramatic increase in work hardening with decreasing temperature as compared to the recrystallized microstructure. Other differences become more apparent when both microstructures are plotted together in figure 13. The unrecrystallized microstructure has a much higher work hardening rate at all temperatures. Additionally, the fully plastic slopes of the unrecrystallized work hardening curves are steeper than their counterparts in the recrystallized microstructure. At 77 K there is a steep drop in the work hardening just before the onset of necking. In both microstructures the 200 K and 300 K curves display very steep curves, although the recrystallized curves have shallower slopes as they reach the necking criterion. The curves at these temperatures raise questions as to whether both microstructures actually become fully plastic. If they do achieve full plasticity at these temperatures, then they experience very short fully plastic states.

3.3.2 Solution Heat Treated

Upon solution heat treatment the work hardening behaviors for both microstructures change significantly. As shown in figure 14, the curves extend over a greater stress range, and their fully plastic regimes are well developed, even at 300 K and 200 K. The curves now break into the fully plastic regime at higher work hardening values, and their temperature dependencies have been reduced. The 200 K curves fall below the 300 K curves. For the unrecrystallized microstructure this dip in work hardening is also reflected in the mechanical properties listed in Table 5.

3.3.3. Effect of Grain Structure

To evaluate the effect of grain structure alone on the work hardening, the unrecrystallized and recrystallized SHT curves are plotted together in figure 15. As mentioned earlier, the solution heat treatment alters the microconstituents but not the grain structure. T_1 is removed, and δ' increases in population but also decreases in size. Therefore, any differences in work hardening after SHT are primarily due to grain structure.

What is most noticeable is the decrease in work hardening between 300 K and 200 K in both microstructures. This drop is also reflected in the mechanical properties in Table 5. Again, the unrecrystallized microstructure has higher work hardening at all temperatures, and the fully plastic slopes are steeper. The unrecrystallized microstructure also continues to show more of a temperature dependence.

3.3.4 Effect of Microconstituents

When the microconstituents are added to the material, i.e., by starting with the SHT condition and then comparing it to the peak-aged (AR) condition, the work hardening changes considerably. When the SHT and AR conditions are plotted at constant microstructure in figure 16, there are several signifcant differences. First, the SHT curves extend over a larger stress range. The biggest differences are at 300 K and 200 K. Adding microconstituent features seems to either drastically shorten the fully plastic regimes at the higher temperatures or prevents the onset of the fully plastic state by satisfying the necking criterion before full plasticity can be established. Second, the transition into the fully plastic state is lowered. Third, the fully plastic slope at 77 K in both microstructures becomes slightly steeper. Fourth, the elastic-plastic slopes also change. For the recrystallized microstructure the slopes become steeper while in the unrecrystallized case, the slopes become shallower, or less negative.

3.3.5 Effect of Grain Structure on Microconstituent Influence on Work Hardening

Comparing the work hardening curves of the two microstructures and the two heat treats at constant temperature aids in assessing the effect of grain structure on the microconstituents' influence on the work hardening. From figure 17 it is apparent that the grain structure has the biggest impact at 77 K. For the unrecrystallized microstructure the

transition point drops significantly with microconstituent additions, and the transition is more gradual in the SHT case. This microstructure also shows a much higher microconstituent dependence with a significant increase in the elastic-plastic slope.

3.4 Surface Relief

Specimens strained to the elastic-plastic regime (0.1-0.5% plastic strain) in figure 18 show very planar and very inhomogeneous slip. Not much surface relief is evident. Specimens strained to the fully plastic regime (3.1±0.3% plastic strain) in figure 19, however, show quite a bit of surface relief. At 77 K there is increased surface roughness, or out-of-plane grain rotation, for both microstructures over those at 300 K. In addition, the unrecrystallized microstructure displays greater surface roughness at both temperatures. This increased roughness has been observed by Glazer[1], Yao, et al.[2], in an earlier production of 2090-T81.

In the fully plastic regime the slip is much more complex. In the grain interiors, multiple slip systems have become activated, and wavy slip is evident as well. Both planar and wavy slip are present to various degrees, and wavy slip is rated on a scale of 1-4 in Table 6 with 1 denoting the highest amount present. The greatest degree of wavy slip is observed in the unrecrystallized 300 K specimen, with the least in the recrystallized 77 K specimen. Near the grain boundaries, slip becomes complicated. There are quite a few phenomena that occur near the boundaries. Many of the various types of grain boundary slip have been documented by Barlow, et al.[31] for cold rolled pure aluminum. The different slip behavior near the boundaries is not surprising since grains must maintain continuity at the boundary.

To define the deformation microstructure in the fully plastic state, the surface deformation was sketched to determine any sort of developing deformation pattern. From the sketch, shown in figure 20, two important observations are evident. First, the deformation occurs in bands, or planes, across the specimen. One band of grains will deform rather heavily while an adjacent band of grains will deform only slightly. Second, the deformation is extremely inhomogeneous. This result is not surprising given the fact that the unrecrystallized microstructure is very inhomogeneous. The inhomogeneity of deformation occurs at two levels: at the granular level and at the intragranular level.

Granular inhomogeneities are reflected by either the existence of grains that show no deformation or the differences in the extent of slip between grains (figure 20). Some grains, on the other hand, show extensive slip while others show very little slip. At the intragranular level the slip can vary from one end of the grain to the other, and the slip spacing and orientation will usually differ near the grain boundary. The different slip at the grain boundary has been well documented, as mentioned above[31]. Also, slip bands can occur in groups. On a more macroscopic scale, more deformation is occurring in the bottom of the sample. No shear bands can be seen in the specimen.

15

Table 6- Scale of the relative amount of wavy slip present in the AR specimens strained to 3.1± 0.1%. They are rated on a scale of 1-4 with 1 indicating the highest amount of wavy slip observed.

Microstructure	300 K	77 K
Unrecrystallized	1	3
Recrystallized	2	4

3.5 Slip Band Analysis

Average slip band spacing measurements taken in the elastic-plastic and fully plastic regions show that the spacing decreases with increasing strain. Strains and their corresponding spacings are listed in Table 7. When slip band spacing is plotted against strain in figure 21, where the dotted lines are drawn to aid in detecting any trends, no trends can be detected. It is expected that those specimens with the highest work hardening rates would have the smallest spacing. The anticipated order from the most homogeneous slip spacing to the least would be 4 K unrecrystallized, 77 K unrecrystallized, 300 K unrecrystallized, 4 K recrystallized, 77 K recrystallized, and finally, 300 K recrystallized. From Table 7 and figures 12 and 21, it is apparent that there is no correlation between surface slip homogeneity and increased work hardening in the strain regime examined.

3.6 Surface Profilometry

Surface profiles for AR specimens strained to 3.1%±0.3% are presented in figure 22. Their corresponding R_a values are given in the figure. The unrecrystallized microstructure does have the greatest amount of surface roughness at both temperatures, but, when compared to the change in roughness with decreasing temperature in the recrystallized microstructure, the recrystallized increases roughness by nearly 36%; the unrecrystallized increases by approximately 6%.

Table 7- The average slip band spacing for each test specimen strained to both the elastic-plastic transition and the fully plastic regions of the work hardening curve.

Temperature [K]	Unrecrystallized Microstructure		Recrystallized Microstructure	
	Strain [%]	Slip Band Spacing [μm]	Strain [%]	Slip Band Spacing [μm]
300	0.4 2.7	7.9 2.4	0.4 3.4	5.7 1.1
77	0.1 3.0	8.8 3.1	0.5 2.8 3.0	3.6 2.7 1.8
4	1.5 3.6	4.1 2.4	1.4 3.1	9.5 2.3

4. DISCUSSION

Due to the complex microstructure of 2090-T81, the influence of microstructure had to be divided into two levels: the grain structure influence and the microconstituent influence. The grain structure consists of grain size, grain shape, subgrains and texture; the microconstituents consist of the precipitate structure and solutes. Since it was first suspected that grain structure was the more likely candidate for the differences in work hardening behavior[3], how an unrecrystallized grain structure alone affected the work hardening differently from the recrystallized was the first question. The next feature to consider was how the microconstituents effected change in the work hardening behavior of both microstructures. Since the microconstituent structure was affected by the grain structure- T_1 did not nucleate equally on all four variant planes- the microconstituent influence could be further divided into two contributions: the grain structure effect on the microconstituent influence and the effect of microconstituents alone. The work hardening curves also pointed out that the elastic-plastic transition region discussed earlier might have been important in influencing the subsequent work hardening behavior.

Because the amount of literature devoted to correlating deformation microstructure observations with work hardening was rather limited, an attempt was made to correlate surface observations with work hardening behavior in the AR material based upon previous work by Jata and Starke[4], Glazer[1] and Yao, et al[2]. Jata and Starke were the first to relate increasing slip homogeneity with increasing work hardening exponent. Then, Yao, et al., suggested the possibility that increasing out-of-plane rotation of surface grains promoted greater slip homogeneity and therefore increased the work hardening rate. What was still unknown in this alloy, however, was the deformation microstructure expected in the fully plastic state, as defined by the θ versus σ curve, of the unrecrystallized microstructure. It would be reasonable to expect that the deformation microstructure would be very inhomogeneous since the microstructure itself had inhomogeneities.

In this section, the effect of temperature, grain structure, and microconstituents will first be considered. Second, the results from these curves will be used to discuss the significance of the elastic-plastic transition region in this alloy. Third, the deformation microstructure of the fully plastic state in the AR unrecrystallized microstructure will be treated. Then, the influence of out-of-plane rotation of surface grains will be assessed, and finally, the relationship between slip homogeneity and work hardening will be addressed.

4.1 Influence of Temperature

It is apparent in figure 13 that with decreasing temperature the slopes of the fully plastic region for all microstructures decrease, in good agreement with Kocks[18]. At the dislocation level it is believed that with a decrease in temperature, thermally activated dynamic recovery processes such as cross slip and dislocation substructure rearrangement do not readily occur. This temperature dependence is accounted for in the second term of the right hand side of equation (1). Some changes in work hardening are therefore

expected with changes in test temperature. Differences in work hardening cannot be solely attributed to temperature changes, and questions as to the precise role of microstructure remain.

4.2 Influence of Microstructure

4.2.1 Influence of Grain Structure

Treatment of the grain structure influence on work hardening in the literature is extremely limited. The KM model predicts linear behavior in the fully plastic state for pure, well annealed FCC materials. It has been generally accepted that grain structure does not play an important role in work hardening in the fully plastic regime; it merely increases the yield strength. What is believed to be important in the fully plastic regime is the interaction of dislocations.

From the solution heat treated data in figure 15, however, grain structure does influence the work hardening behavior. The unrecrystallized grain structure breaks into the fully plastic regime at a higher work hardening rate than the recrystallized grain structure. The work hardening rates are consistently higher early in the fully plastic regime, although there is some inconsistency in this behavior at the later stages. This unrecrystallized grain structure also has a steeper fully plastic slope but a shallower elastic-plastic slope. The combination of a shallow elastic-plastic slope and a steep fully plastic slope seems, in general, to decrease the uniform elongation. When comparing the two grain structures at the same heat treatment condition, there is a general tendency for the uniform elongation to increase with a steep elastic-plastic slope and a shallow fully plastic slope. There is, however, an exception with the 200 K condition in both grain structures. The drop in the work hardening rate at 200 K after SHT is unusual. There are two possible explanations. First, another mechanism may be dominating at this temperature. Or second, dynamic strain aging is occurring at 300 K for both microstructures, especially in the unrecrystallized microstructure. The specimens are in the as-quenched condition. At 300 K the diffusion rates of solutes and vacancies are higher, and they may be clustering at dislocations, thus providing a drag force that retards dislocation motion.

4.2.2 Influence of Microconstituents on Work Hardening

4.2.2.1 Grain Structure Effects on Microconstituent Influence

The grain structure plays an important role in the development of the microconstituents. To evaluate the influence of grain structure on microconstituents, all work hardening curves can be plotted at constant temperature, shown in figure 17. Comparison of the fully plastic behavior at 300 K and 200 K may not be valid since there is some question as to whether the fully plastic state is reached at these temperatures; this issue will be discussed in the next section. The grain structure has the strongest influence at 77 K. The transition into the fully plastic state drops much more dramatically for the unrecrystallized microstructure. The grain structure also seems to affect the elastic-plastic

19

slope at 300 K and 77 K. The unrecrystallized microstructure causes a more negative elastic-plastic slope with the addition of microconstituents. The recrystallized microstructure has the opposite effect. Consequently, the grain structure affects both regimes of the work hardening behavior: the elastic-plastic regime at both high and low temperatures, and the fully plastic regime at low temperatures.

4.2.2.2 Microconstituent Effects

When microconstituents are added to the SHT specimens, the most noticeable change is in the 200 K and 300 K conditions, as can be seen in figure 16. The "fully plastic" regions are barely perceptible, if they are present at all, and there is some question as to whether the material has actually achieved the fully plastic condition. There are two equally viable interpretations: they are fully plastic, but for a very short stress range, or they never achieve full plasticity due to the early onset of the necking criterion.

In the former case there could be two competing mechanisms: the matrix friction stress and the precipitate stress; the situation is depicted schematically in figure 23. At higher temperatures the friction stress is low enough such that dislocation motion is relatively uninhibited by the matrix. Dislocation motion is, however, impeded by the precipitates, where the dislocation must shear through δ', cross slip over T_1, or tangle. As the temperature decreases, the matrix friction stress will rise and dislocation motion becomes heavily influenced by this stress. The difficulty for a dislocation to travel through the matrix outweighs the dislocation's encounter with a precipitate, thus shortening the stress range of the fully plastic regime.

In the latter case it is plausible that at the higher temperatures it is not possible to attain the fully plastic state. The addition of the microconstituents hardens the matrix in the 300 K and 200 K conditions such that the material fulfills the necking criterion before it even reaches the fully plastic state. 2090 in the peak-aged condition contains fully developed δ'. δ' is known to localize slip because it relies upon order strengthening. In the SHT case, the smaller size of δ' probably reduces its effectiveness in retarding dislocation motion. Therefore, slip localization should not be as prevalent, and slip will be more homogeneous. As a consequence, the elongation increases and the strength decreases, and the material can become fully plastic.

Another point to note is that just before the onset of necking, both microstructures show a steep drop in the work hardening rate at 77 K. When the work hardening rate is plotted versus true strain, shown in figure 24, a sudden drop in the work hardening rate occurs just before the two curves intersect. In the solution heat treated case, however, this drop is not seen. Previous work has shown that no significant change in fracture mode occurs with decreasing temperature[3] in either microstructure. The sudden drop may be due to the localization of strain by the presence of peak-aged δ'. After solution heat treatment, δ' may not be as effective in promoting planar slip.

20

4.2.3 Summary

The unrecrystallized microstructure provided the highest rate of work hardening at all temperatures and heat treatment conditions. The unrecrystallized grain structure also had the shallower elastic-plastic slopes but steeper fully plastic slopes. The grain structure effect on the microconstituents influenced the value of the work hardening rate at which the transition into the fully plastic state occurred. That value dropped more dramatically with the addition of microconstituents for the unrecrystallized grain structure at 77 K. In addition, the unrecrystallized microstructure caused the elastic-plastic slope to become more negative with the addition of microconstituents while the recrystallized microstructure had the opposite effect. Therefore, the grain structure affected both the elastic-plastic and the fully plastic regions of the work hardening plot. Finally, the addition of microconstituents alone had one of two possible effects. Either they hardened the matrix such that full plasticity was not achieved at 200 K and 300 K, or the effect of microconstituents was to shorten the fully plastic regime.

4.3 Importance of the Elastic-Plastic Transition Region

According to the KM model, the elastic-plastic transition region is not important to the work hardening of a well annealed FCC material because the amount of strain that occurs in this region is very small. The results of this study have shown that alterations of the microstructure in 2090-T81 (figures 15 and 16), regardless of the microstructure, affect the slope of this region. Even though this region may cover a small range of the uniform elongation, there is a sharp drop in the work hardening rate. A majority of the work hardening rate is lost in this region. In addition, the development of the deformation microstructure begins near yielding. What structure evolves at this stage most certainly could affect the later deformation behavior.

The effect of microstructure on the slopes of a work hardening curve can be examined more quantitatively by fitting two lines to the curve, one for the elastic-plastic transition and one for the fully plastic regime, as depicted in figure 25. The equation for the line in either regime is simply

$$\theta = m\sigma + b.$$

b can be solved by the condition $\theta(0) = \theta_0$, where θ_0 is the intercept. Thus, the equation can be written as

$$\theta = m\sigma + \theta_0. \tag{2}$$

θ_0 can be expressed in terms of true stress by considering the condition $\theta(\sigma_s) = 0$; σ_s is the stress value when the work hardening rate equals zero. Then,

$$0 = m\sigma_s + \theta_o$$

and

$$\theta_o = -m\sigma_s.$$

Substituting this value into equation (2) gives

$$\theta = m\sigma - m\sigma_s$$

$$= m(\sigma - \sigma_s).$$

By integrating this expression, the calculated elongation for each region may be calculated by the equation

$$\varepsilon = \frac{1}{m}\ln\left(\frac{\sigma - \sigma_s}{\sigma_y - \sigma_s}\right)$$

where σ_y is the yield strength. If σ is the strength at necking, where equation (2) can be solved for the condition $\theta = \sigma$, then ε is the uniform elongation attained if the work hardening were due solely to a single regime- either elastic-plastic or fully plastic.

The ideal uniform elongation of a material can be calculated by determining the amount of expected elongation due to the elastic-plastic regime (from σ_y to σ_i in figure 25) and then evaluating the amount of expected elongation due to the plastic regime alone (σ_i to σ_n in figure 25), and then summing the two contributions. It is suspected that with a steeper elastic-plastic slope, a material is able to attain more elongation in the fully plastic region. For example, in 2090, a change in microstructure, from AR unrecrystallized to AR recrystallized at 77 K steepens the elastic-plastic slope by two times. If $-m_{ep}$ is the slope of the unrecrystallized microstructure in the elastic-plastic region, then $-2m_{ep}$ is the corresponding slope of the elastic-plastic region in the recrystallized microstructure. Also, the fully plastic slope becomes less negative; if $-0.06m_{ep}$ is the slope of the unrecrystallized microstructure in the plastic region, then $-0.02m_{ep}$ is the plastic slope of the recrystallized microstructure. All of these variables can be expressed in terms of the unrecrystallized elastic-plastic variables; they are listed in Table 8. Based upon equation (2), four equations, two for each microstructure and one for each region, can be written as

$$\theta_{ep}^{unrx} = -m_{ep}\sigma + \theta_{ep}^o$$

$$\theta_p^{unrx} = -0.06m_{ep}\sigma + 0.09\theta_p^o$$

$$\theta_{ep}^{rx} = -2m_{ep}\sigma + 1.46\theta_{ep}^{o}$$

$$\theta_{p}^{rx} = -0.02m_{ep}\sigma + 0.03\theta_{p}^{o} .$$

σ_i for each microstructure can be solved by setting $\theta_{ep} = \theta_p$. σ_n, the strength at necking, can be solved by utilizing the necking condition $\theta = \sigma$ in equation (2). As seen in Table 8, all stresses are in terms of the yield strength for the unrecrystallized microstructure. Thus, the strain contributions for the elastic-plastic and the fully plastic regions are, respectively, the general equations

$$\varepsilon_{ep} = \frac{1}{m}\ln\left(\frac{\sigma_i - \sigma_s}{\sigma_y - \sigma_s}\right)$$

$$\varepsilon_{p} = \frac{1}{m}\ln\left(\frac{\sigma_n - \sigma_s}{\sigma_i - \sigma_s}\right) .$$

Table 8- Variables for calculating the ideal uniform elongation. All variables are given in terms of the unrecrystallized microstructure elastic-plastic slope, the unrecrystallized microstructure yield strength, and the unrecrystallized microstructure work hardening rate intercept.

	m	σ_y	θ_o	σ_i	σ_s	σ_n
Unrecrystallized elastic-plastic	$-m_{ep}$	σ_y	θ_{ep}^{o}	$1.19\sigma_y$	$1.23\sigma_y$	
Unrecrystallized plastic	$-0.06m_{ep}$	σ_y	$0.09\theta_{ep}^{o}$	$1.19\sigma_y$	$1.73\sigma_y$	$1.48\sigma_y$
Recrystallized elastic-plastic	$-2m_{ep}$	$0.80\sigma_y$	$1.46\theta_{ep}^{o}$	$0.89\sigma_y$	$0.90\sigma_y$	
Recrystallized plastic	$-0.02m_{ep}$	$0.80\sigma_y$	$0.03\theta_{ep}^{o}$	$0.89\sigma_y$	$1.82\sigma_y$	$1.19\sigma_y$

The four strain equations are

$$\varepsilon_{ep}^{unrx} = -\frac{1}{m_{ep}}\ln\left(\frac{1.19\sigma_y - 1.23\sigma_y}{\sigma_y - 1.23\sigma_y}\right) = 1.75m_{ep}^{-1}$$

$$\varepsilon_{p}^{unrx} = -\frac{1}{0.06m_{ep}}\ln\left(\frac{1.48\sigma_y - 1.73\sigma_y}{1.19\sigma_y - 1.73\sigma_y}\right) = 12.84m_{ep}^{-1}$$

$$\varepsilon_{ep}^{rx} = -\frac{1}{2m_{ep}}\ln\left(\frac{0.89\sigma_y - 0.90\sigma_y}{0.80\sigma_y - 0.90\sigma_y}\right) = 1.15m_{ep}^{-1}$$

$$\varepsilon_{p}^{rx} = -\frac{1}{0.02m_{ep}}\ln\left(\frac{1.19\sigma_y - 1.82\sigma_y}{0.89\sigma_y - 1.82\sigma_y}\right) = 19.47m_{ep}^{-1}$$

then, the calculated uniform elongations, which are the sum of both regions, are

$$\varepsilon_{ue}^{unrx} = 14.59m_{ep}^{-1}$$

$$\varepsilon_{ue}^{rx} = 20.62m_{ep}^{-1}.$$

For 2090, then, a more negative elastic-plastic slope at 77 K by a factor of two from the unrecrystallized to recrystallized microstructure results in approximately a 40% increase in elongation. In addition, the plastic slope becomes 34% less negative.

4.4 Fully Plastic State

The fully plastic state was purely a theoretical construct, and little work had gone into defining the microstructural response and resulting deformation pattern. Because there was some question as to whether the higher temperature specimens had achieved the fully plastic state in the AR condition, it was necessary to define the plastic state of this alloy on a microstructural level. Then, future questions pertaining to the achievement of full plasticity could be based upon this fully plastic surface deformation pattern.

The first step was to examine the surface deformation pattern of the unrecrystallized microstructure in the middle of the fully plastic regime (figure 20). The observed bands of deformation are not surprising in light of the type of grain structure found in this material. The pancake shaped grains can essentially be considered as a deck of cards. When the "deck" of grains is sheared, most bands will deform, but a few will not. Even among those that do deform, the amount of deformation will vary from band to band. Initially, when the material is being pulled in tension, isolated grains with the most favorable orientations will yield first. As deformation increases, the grains surrounding these grains will begin to deform. Eventually, in the plastic state, there are still some grains that either have not yet yielded, or they were one of the last to yield. The concentration of lightly deformed or undeformed grains near the top of the specimen may indicate that the top of the

specimen is harder than the bottom. Yield strength gradients will occur through the specimen due to the deformation gradients set up by the rolling process.

Therefore, the deformation microstructure of the fully plastic state in the unrecrystallized AR microstructure will appear very inhomogeneous. The inhomogeneity will exist both at the granular level and at the intragranular level. In addition, the deformation of grains will occur in bands. It is unknown what the inhomogeneity of deformation in the fully plastic region implies. It is known that deformation in the grain interior differs from the deformation at the boundary[21,22,31]. Strain compatibility near the grain boundaries is maintained by activating additional slip systems. Inhomogeneous deformation may be a consequence of the deformation process and will not influence work hardening.

4.5 Work Hardening and Surface Roughness

In previous work[1,2] on Vintage I 2090-T81, out-of-plane rotation of grains and subgrains on the surface were observed when the test temperature decreased from 300 K to 77 K. It was suggested that this out-of-plane rotation resulted from the difficulty of transmission of slip from grain to grain[2]. Consequently, the work hardening increased with decreasing temperature. In Vintage III, however, it was found that there was a greater increase in out-of-plane rotation in the recrystallized microstructure with decreasing temperature, by as much as 36%, yet this microstructure had the smaller increase in work hardening. Thus, out-of-plane grain rotation did not directly correlate with the dramatic increase in work hardening in this vintage.

4.6 Work Hardening and Homogeneity of Slip Band Spacing

The lack of correlation between finer slip band spacing, or more homogeneous slip, and increased work hardening is surprising. It is usually expected that finer slip spacing, or increased slip homogeneity, is a sign of a higher work hardening rate, since the deformation is not localized. Jata and Starke have found that finer slip spacing in 2090 corresponds to better fracture toughness and increased strain hardening exponent (n). An increasing n value implies an increased work hardening rate. There are difficulties associated with this parameter since it is an average over much of the stress-strain curve, and it is sensitive to the method of its determination.

Some difficulties may arise from relating the slip band spacing of the surface to the work hardening. The surface grains are under different constraint conditions than the interior grains, thus they may deform differently from the interior grains. Barlow, et al.[31], have found that the deformation microstructures near the grain boundaries in the interior of the specimen correlated well with the surface deformation microstructures. The incidence of structures found on the surface is less than those found in the interior. If the surface slip analysis is consistently utilized to assess work hardening for all test conditions, then the surface could be a valid measurement for comparison purposes.

In addition, the occurrence of wavy slip, usually indicative of homogeneous slip, is highest in the unrecrystallized microstructure, yet the unrecrystallized microstructure has the highest work hardening rate. Recall that cross slip is considered a recovery process and that an increase in cross slip usually denotes a lower work hardening rate. The higher amount of cross slip in the unrecrystallized microstructure may reflect the higher amount of stress this microstructure experiences. The cross slip then results from mechanically activated processes instead of thermally activated ones.

5. CONCLUSIONS

The effect of grain structure and microconstituents on work hardening behavior in aluminum alloy 2090-T81 was investigated. Efforts were made to relate increasing surface roughness and slip homogeneity with increasing work hardening. The increase in out-of-plane rotation of grains and subgrains was not found to be primarily responsible for increasing the work hardening rate. Surface roughness measurements revealed that with decreasing temperature, the recrystallized microstructure, which had the smallest increase in work hardening with decreasing temperature, had the greatest increase in R_a value, i.e., the greatest amount of grain rotation. The difficulty of transmission of slip from grain to grain did not contribute to the increase in work hardening seen in the unrecrystallized microstructure. The work hardening rate was also not a function of slip homogeneity. No correlation was found between increasing surface slip homogeneity and increasing work hardening for either microstructure. Therefore, slip homogeneity was not the only important feature in increasing the work hardening rate.

Additional surface observations provided a means of defining the deformation microstructure of the fully plastic state of the unrecrystallized microstructure. At 77 K the unrecrystallized microstructure had very inhomogeneous surface deformation, and the deformation appeared to occur in planes, or bands. The deformation pattern indicated that grains yielded in groups throughout the thickness of the specimen. These bands of deformed grains surrounded bands of grains that had very slight or no deformation.

Due to the interrelationship between the many variables: solutes, precipitates, texture, subgrains and initial dislocation substructure, isolating one particular microstructural feature was difficult. Instead, the effect of microstructure had to be divided into two levels: the influence of grain structure (texture, grain shape and size, and subgrains) and the influence of microconstituents (precipitate structure and solutes). It was found that an unrecrystallized, {110}<112> textured grain structure with a homogeneous distribution of subgrains had the highest level of work hardening over the temperature range between 300 K and 77 K when compared to a recrystallized, textured grain structure with an inhomogeneous distribution of subgrains. With the addition of microconstituents, the elastic-plastic slopes at high and low temperatures and the fully plastic slope at low temperatures of both microstructures were affected. The unrecrystallized microstructure caused a more negative elastic-plastic slope at 300 K and 77 K, and the recrystallized microstructure had the opposite effect. Thus, the elastic-plastic transition region might be important to the work hardening behavior of this material. Also, the work hardening level at which the unrecrystallized microstructure transitioned from elastic-plastic to fully plastic dropped much more dramatically than the drop for the recrystallized microstructure. The fully plastic slope for both microstructures became more negative with the addition of microconstituents. When considering the effect of microconstituents alone, the removal of the microconstituents caused the work hardening curves at 200 K and 300 K to achieve well developed, fully plastic states.

27

REFERENCES

1. Glazer, J., *The Strength-Toughness Combination of the Aluminum-Lithium Alloys 2090 and 2091 at Cryogenic Temperatures*, Ph.D. Dissertation, LBL-27607, Berkeley, CA, July, 1989.

2. Yao, D., D. Chu and J.W. Morris, Jr., "Tensile Deformation of Al-Cu-Li-Zr Alloy 2090-T8E41 at 298 and 77K," **Light Weight Alloys for Aerospace Applications**, ed. E.W. Lee, TMS, Warrendale, 1991.

3. Chu, D., *Cryogenic Mechanical Behavior of Vintage III Aluminum-Copper-Lithium Alloy 2090-T81*, M.S. Thesis, LBL-30170, Berkeley, CA, December 1990.

4. Jata, K.V. and E.A. Starke, "Fracture Toughness of Al-Li-X Alloys at Ambient and Cryogenic Temperatures," *Scripta Metall.*, vol. 22, 1988, pp. 1553-1556.

5. Glazer, J., S.L. Verzasconi, E.N.C. Dalder, W. Yu, R.A. Emigh, R.O. Ritchie and J.W. Morris, Jr., "Cryogenic Mechanical Properties of Al-Cu-Li-Zr Alloy 2090," *Adv. Cryogenic Eng.*, vol. 32, 1986, pp. 397-404.

6. Glazer, J., J.W. Morris, Jr., S.A. Kim, M.W. Austin, and H.M. Ledbetter, "Temperature Variation of the Elastic Constants of Aluminum Alloy 2090-T81," *AIAA Journal*, vol. 25, 1987, pp. 1271-1272.

7. Dorward, C., "Cryogenic Toughness of Al-Cu-Li Alloy AA 2090," *Scripta Metall.*, vol. 20, 1986, pp. 1379-1383.

8. Glazer, J., S.L. Verzasconi, R.R. Sawtell and J.W. Morris, Jr., "Mechanical Behavior of Aluminum-Lithium Alloys at Cryogenic Temperatures," *Metall. Trans. A*, vol. 18A, 1987, pp. 1695-1701.

9. Venkateswara Rao, K.T., W. Yu and R.O. Ritchie, "Cryogenic Toughness of Commercial Aluminum-Lithium Alloys: Role of Delamination Toughening," *Metall. Trans. A*, vol. 20A, 1989, pp. 485-497.

10. Venkateswara Rao, K.T., F.H. Hayashigatani, W. Yu and R.O. Ritchie, "On the Fracture Toughness of Aluminum-Lithium Alloys at Ambient and Cryogenic Temperatures," *Scripta Metall.*, vol. 22, 1988, pp. 93-96.

11. Gayle, F.W., "The Development of Aluminum-Lithium Alloys," Reynolds Metals Company Report, July, 31, 1980.

12. Miyasato, S.M., *Early Microstructural Evolution and Deformation Behavior in Solution Heat Treated Aluminum-Lithium Alloys*, Ph.D. Dissertation, December, 1990.

13. Starke, Jr., E.A. and W.E. Quist, " ," *AGARD Conference Proceedings No. 444- New Light Alloys*, AGARD, Essex, England, 1989.

14. Rioja, R.J., P.E. Bretz, R.R. Sawtell, W.H. Hunt and E.A. Ludwiczak, "Precipitation Reactions, Strength and Toughness of Al-Li-Cu Alloys," **Aluminum Alloys- Physical and Mechanical Properties**, 1985, pp. 1781-1797.

15. Gregson, P.J. and H.M. Flower, "Microstructural Control of Toughness in Aluminum-Lithium Alloys," *Acta Metall.*, vol. 33, 1985, pp. 527-537.

16. Howe, J.M., D.E. Laughlin and A.K. Vasudévan, "A High Resolution Transmission Electron Microscopy Investigation of the δ'-θ' Precipitate Structure in an Al-2 wt% Cu Alloy," *Phil. Mag.*, vol. 57, 1988, pp. 955-969.

17. Kim, N.J. and E.W. Lee, "Effect of T_1 Precipitate on the Anisotropy of Al-Li Alloy 2090," *Acta Metall. Mater.*, vol. 41, 1993, pp. 941-948.

18. Kocks, U.F., "Laws for Work-Hardening and Low-Temperature Creep," *Transactions of the ASME: Journal of Engineering Materials and Technology*, January, 1976, pp. 76-85.

19. Mecking, H. and U.F. Kocks, "Kinetics of Flow and Strain-Hardening," *Acta Metall.*, vol. 29, 1981, pp. 1865-1875.

20. Taylor, G.I., "Plastic Strain in Metals," *J. Inst. Metals*, vol. 62, 1938, pp. 307-323.

21. Ashby, M.F., "The Deformation of Plastically Non-homogeneous Materials," *Phil .Mag.*, vol. 21, 1970, pp. 399-424.

22. Thompson, A.W., "Polycrystal Hardening," **Work Hardening in Tension and Fatigue**, ed. A.W. Thompson, TMS-AIME, New York, 1975, pp. 89-126.

23. Thompson, A.W. and M.I. Baskes, "The Influence of Grain Size on the Work Hardening of Face-Centred Cubic Polycrystals," *Phil. Mag.*, vol. 28, 1973, pp. 301-308.

24. Kocks, U.F., "Kinetics of Solution Hardening," *Metall. Trans. A*, vol. 16A, December, 1985, pp. 2109-2129.

25. Haasen, P., "Structural Defects in Solid Solutions," **Alloying Behavior and Effects in Concentrated Solid Solutions**, vol. 29, ed. T.B. Massalski, Gordon and Breach Science Publishers, New York, 1965, pp. 270-294.

26. Hornbogen, E. and K-H. Zum Gahr, "Distribution of Plastic Strain in Alloys Containing Small Particles," *Metallography*, vol. 8, 1975, pp. 181-202 .

27. Honeycombe, R.W.K., **The Plastic Deformation of Metals**, Edward Arnold (Publishers) Ltd., London, 1984.

28. Estrin, Y. and H. Mecking, "A Unified Phenomenological Description of Work Hardening and Creep Based on One-Parameter Models," *Acta Metall.*, vol. 32, 1984, pp. 57-70.

29. Mecking, H., B. Nicklas, N. Zarubova and U.F. Kocks, "A 'Universal' Temperature Scale for Plastic Flow," *Acta Metall.*, vol. 34, 1986, pp. 527-535.

30. Mecking, H., "Description of Hardening Curves of FCC Single and Polycrystals," **Work Hardening in Tension and Fatigue**, ed. A.W. Thompson, TMS-AIME, New York, 1975, pp. 67-88.

31. Barlow, C.Y.J., B. Bay and N. Hansen, "A Comparative Investigation of Surface Relief Structures and Dislocation Microstructures in Cold-Rolled Aluminium," *Phil. Mag. A*, vol. 51, 1985, pp. 253-275.

APPENDIX A. DERIVATION OF THE KOCKS-MECKING EQUATION.

The Kocks-Mecking model[18,19] begins with the assumption that the dislocation-dislocation interaction is the controlling feature in work hardening. The dislocations of particular interest are mobile dislocations that are stored in the crystal and act as obstacles to other dislocations. The relevant parameter, then, is the dislocation density. If σ is the flow stress due to these dislocation obstacles, then

$$\sigma = \alpha\mu b\rho^{1/2} \tag{i}$$

where
α = proportionality constant of order 1,
μ = shear modulus,
b = Burgers vector, and
ρ = dislocation density.

The change in dislocation density during deformation can be written as

$$d\rho = d\rho_{storage} - d\rho_{recovery}. \tag{ii}$$

The first term in (ii) is the dislocation storage rate, and it describes the change in that fraction of the mobile dislocation density ρ_m that has been stored in the crystal after moving a distance dx. This term is given by

$$d\rho_{storage} = \frac{\rho_m}{L} dx \tag{iii}$$

where L = mean free path = $\dfrac{\beta}{\rho^{1/2}}$. $\qquad$ (iv)

The second term in (ii) is related to dynamic recovery and can be expressed as a function of the number of potential recovery sites in an elemental area (da) of a slip plane ρda, the average length L_a of a dislocation that gets annihilated or becomes ineffective, and the volume affected V, in the following manner:

$$d\rho_{recovery} = \frac{L_A \rho\, da}{V}. \tag{v}$$

An increment of strain dε can be expressed as

31

$$d\epsilon = \rho_m b dx = \frac{b}{V} da, \qquad\qquad\text{(vi)}$$

assuming that the probability of a recovery event is proportional to how often a moving dislocation contacts a potential recovery site. Now, by combining equations (ii)-(vi),

$$d\rho = \frac{\rho_m}{L} dx - \frac{L_A}{V} \rho\, da$$

$$= (\rho_m dx)\left(\frac{\rho^{1/2}}{\beta}\right) - L_A \rho\left(\frac{da}{V}\right)$$

$$= \left(\frac{1}{b} d\epsilon\right)\left(\frac{\rho^{1/2}}{\beta}\right) - L_A \rho\left(\frac{1}{b} d\epsilon\right)$$

The change in dislocation density with an increment in strain is now

$$\frac{d\rho}{d\epsilon} = \frac{1}{b\beta} \rho^{1/2} - \frac{L_A}{b} \rho.$$

The derivative of equation (i) with respect to the dislocation density is

$$\frac{d\sigma}{d\rho} = \frac{\alpha\mu\beta}{2\rho^{1/2}}.$$

Then

$$\frac{d\sigma}{d\epsilon} = \frac{d\sigma}{d\rho}\frac{d\rho}{d\epsilon}$$

$$= \left(\frac{\alpha\mu b}{2}\rho^{-1/2}\right)\left(\frac{1}{b\beta}\rho^{1/2}\right) - \left(\frac{\alpha\mu b}{2}\rho^{-1/2}\right)\frac{L_A}{b}\rho$$

$$= \frac{\alpha\mu}{2\beta} - \frac{L_A}{2b}(\alpha\mu b\rho^{1/2})$$

$$= \theta_0 - k_2\sigma$$

where θ_0 is the athermal hardening term, and the second term is the dynamic recovery term where $k_2 = \frac{L_A}{2b}$.
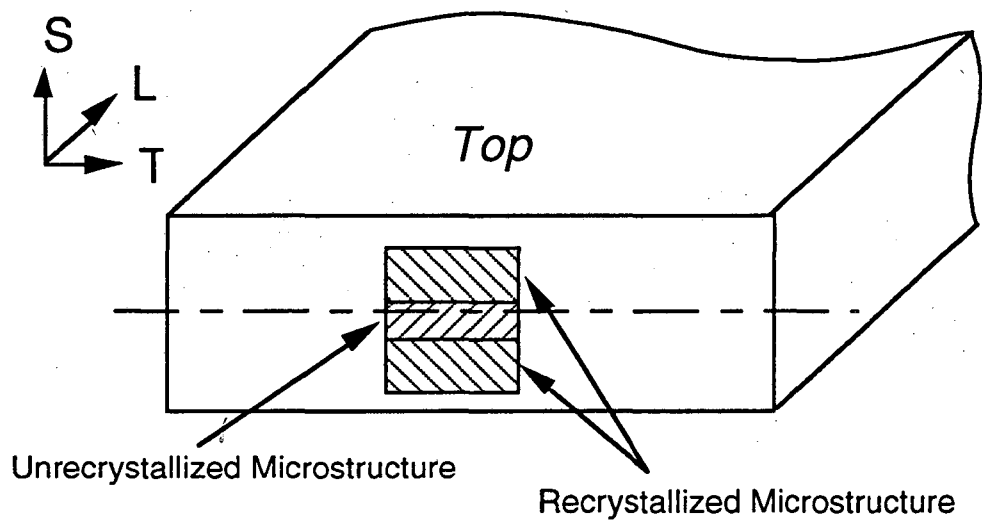
Figure 1. Schematic illustration of the location of both microstructures in the 12.7 mm
plate of 2090-T81. Note that the center of the unrecrystallized microstructure is
not the geometrical center of the plate.
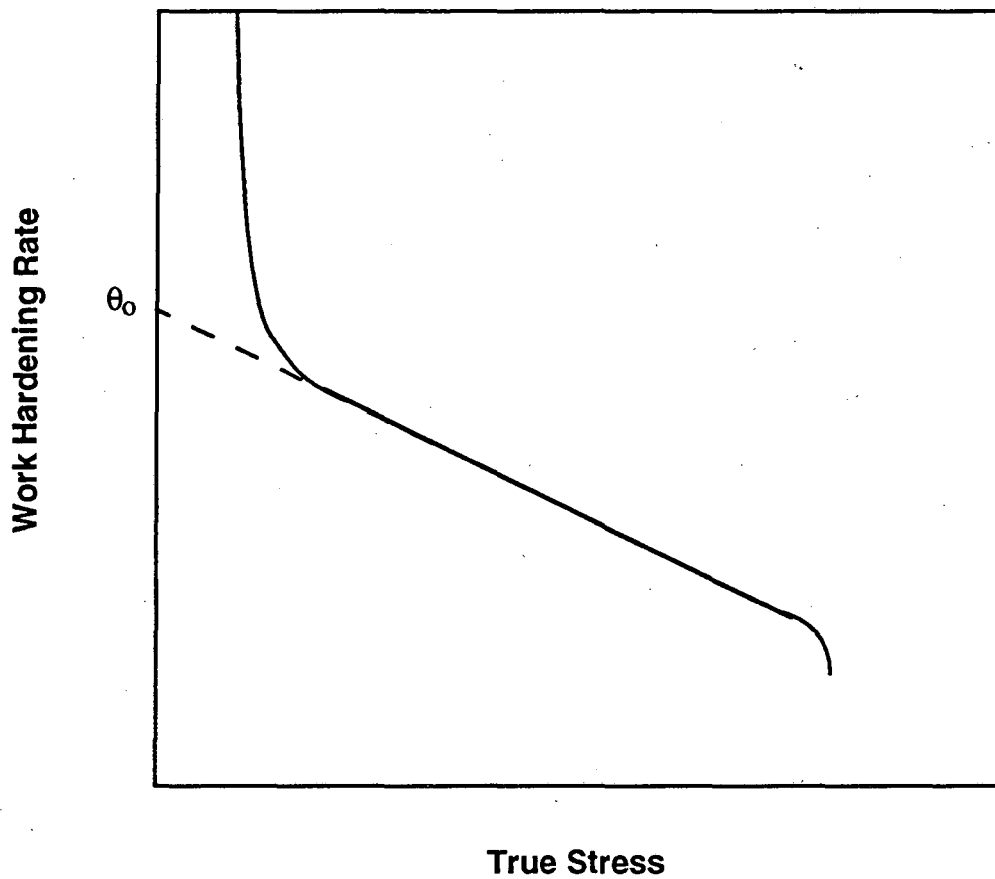
Figure 2. Diagram of the Kocks-Mecking model. The linear portion extrapolates to a constant value θ_0 at zero stress.
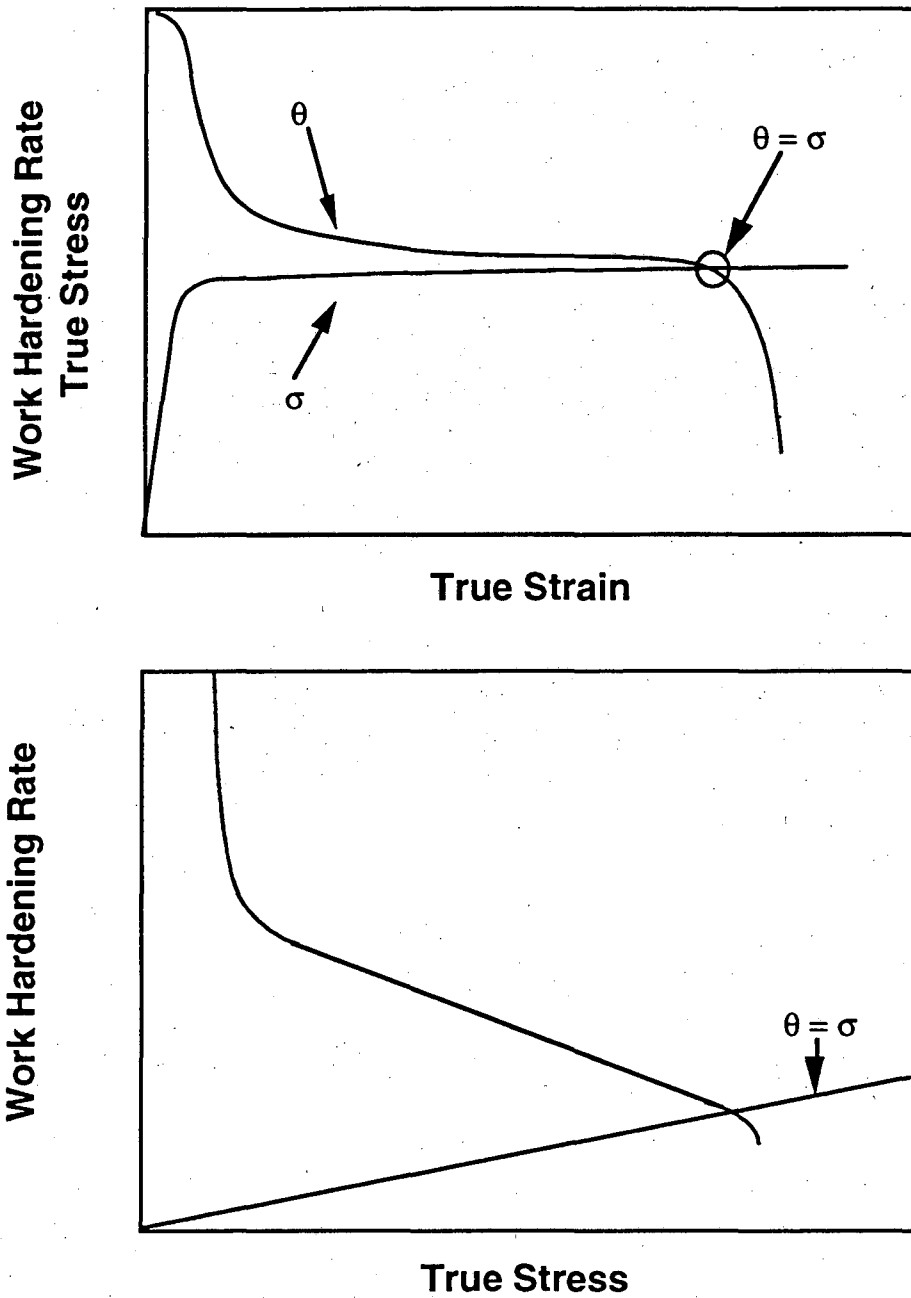
Figure 3. Work hardening rate (θ) plotted versus true strain (top) and versus true stress (σ) (bottom). The necking criterion $\theta = \sigma$ is indicated in each plot.
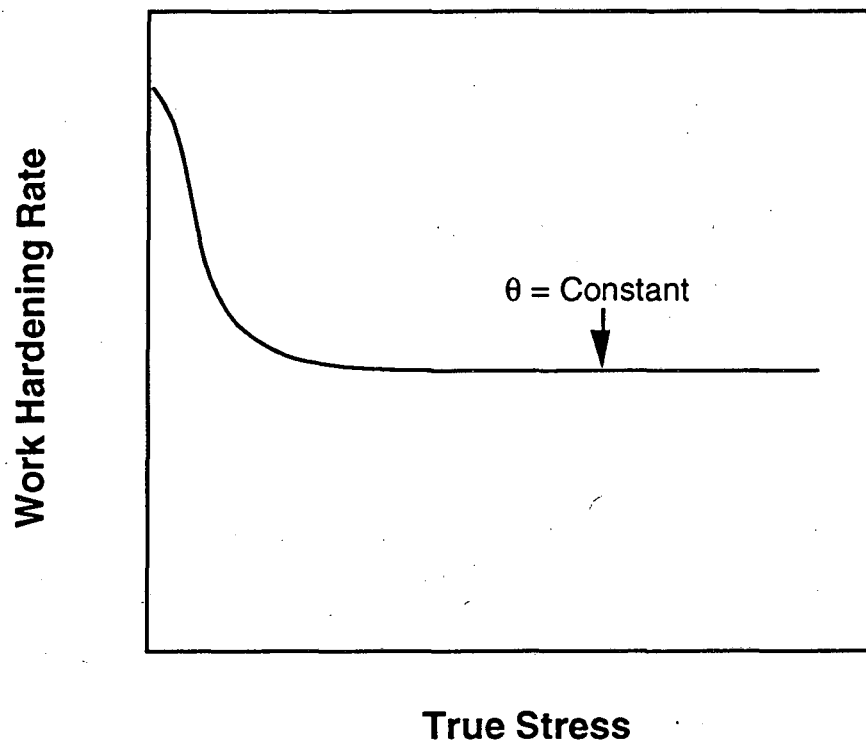
Figure 4. The ideal work hardening curve has a region of constant work hardening where θ = Constant[30]
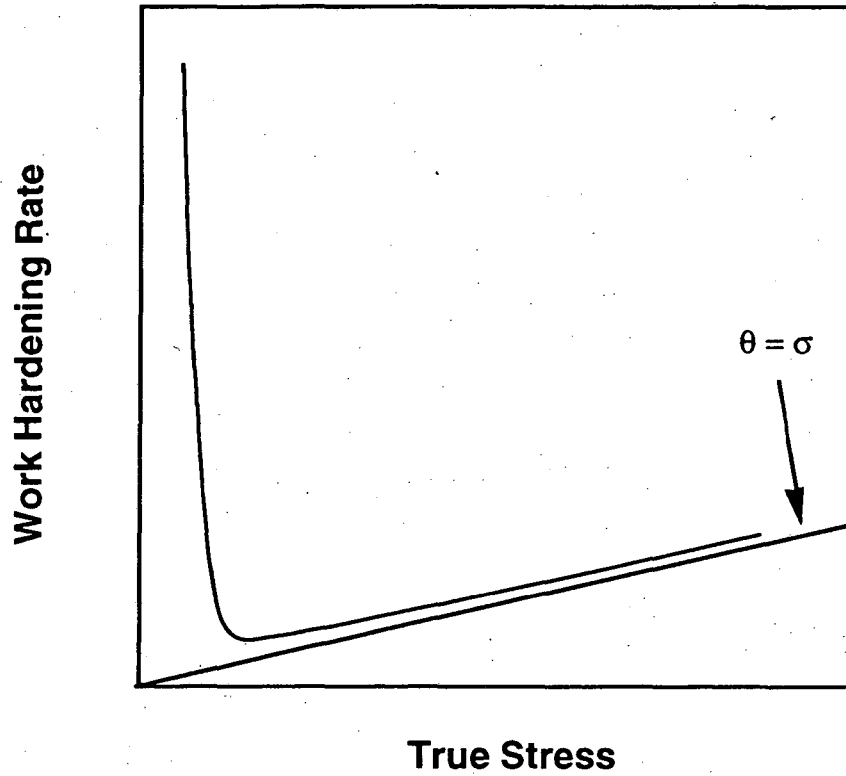
Figure 5. Ideal work hardening behavior for a material undergoing hardening and recovery processes. The work hardening rate maintains a value slightly higher than the necking criterion ($\theta = \sigma$).

a) $m_1 < m_2$

b) $\theta_2^o < \theta_1^o$
$\theta_2^{'} < \theta_1^{'}$

c) $\theta_1 > \theta_2$

True Stress
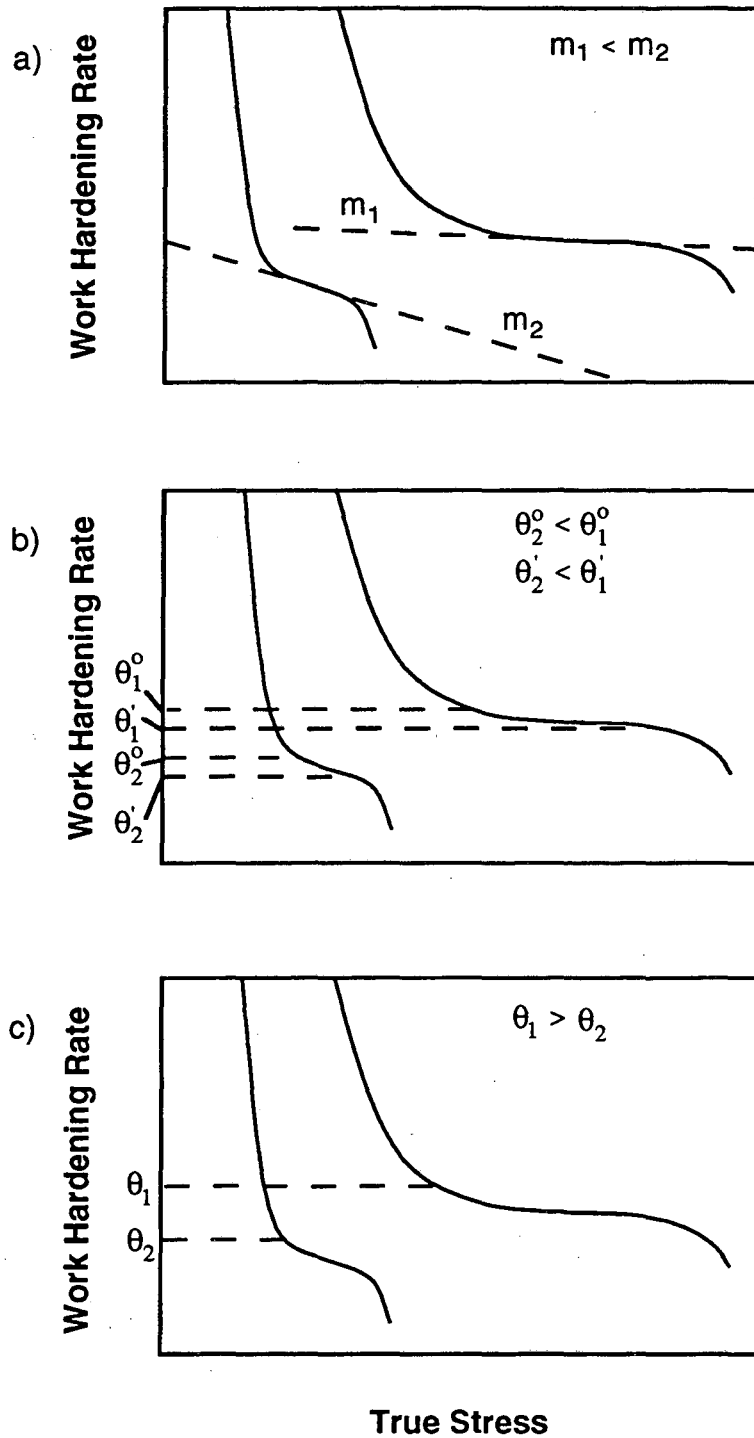
Figure 6. Significant characteristics of the work hardening curve: a) the slopes of the fully plastic regions (m_1, m_2); b) the level of the work hardening rate in the fully plastic region $(\theta^o, \theta^{'})$; and c) where the transition from elastic-plastic to fully plastic behavior occurs (θ_1, θ_2).
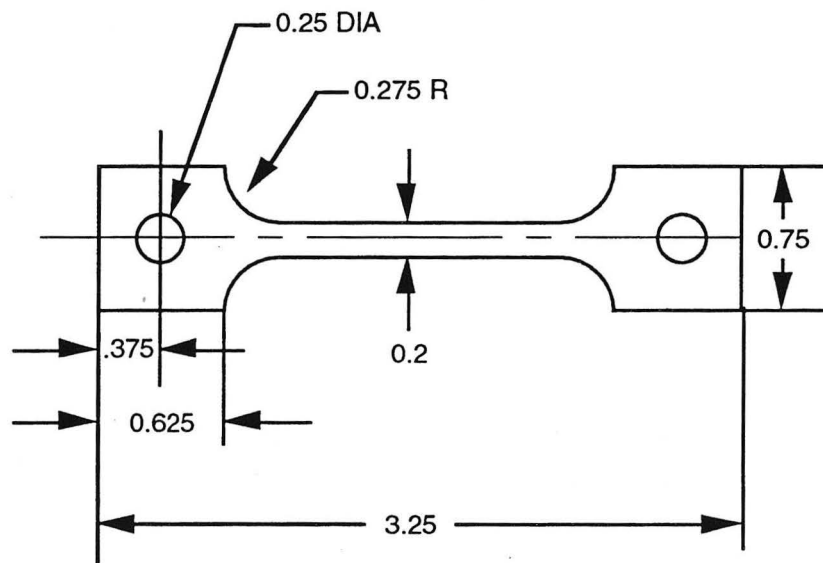
Figure 7. Dimensions of tensile specimens used in this investigation. All dimensions are in inches. Scale ~ 1:1.

100 μm
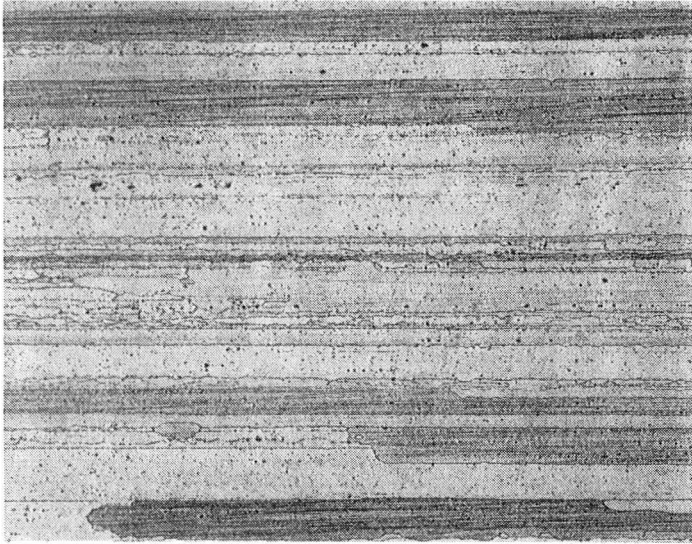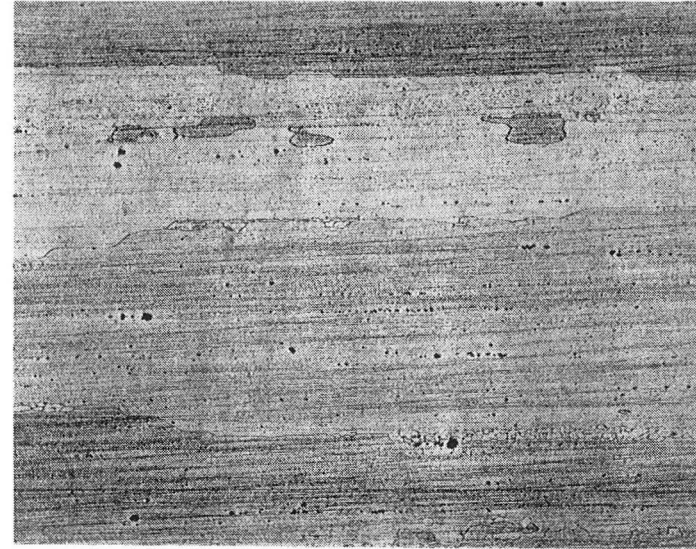
Unrecrystallized   Recrystallized

Figure 8. Optical micrographs of both grain structures. The unrecrystallized microstructure has much thinner grains than the recrystallized microstructure.

XBB 928-6055
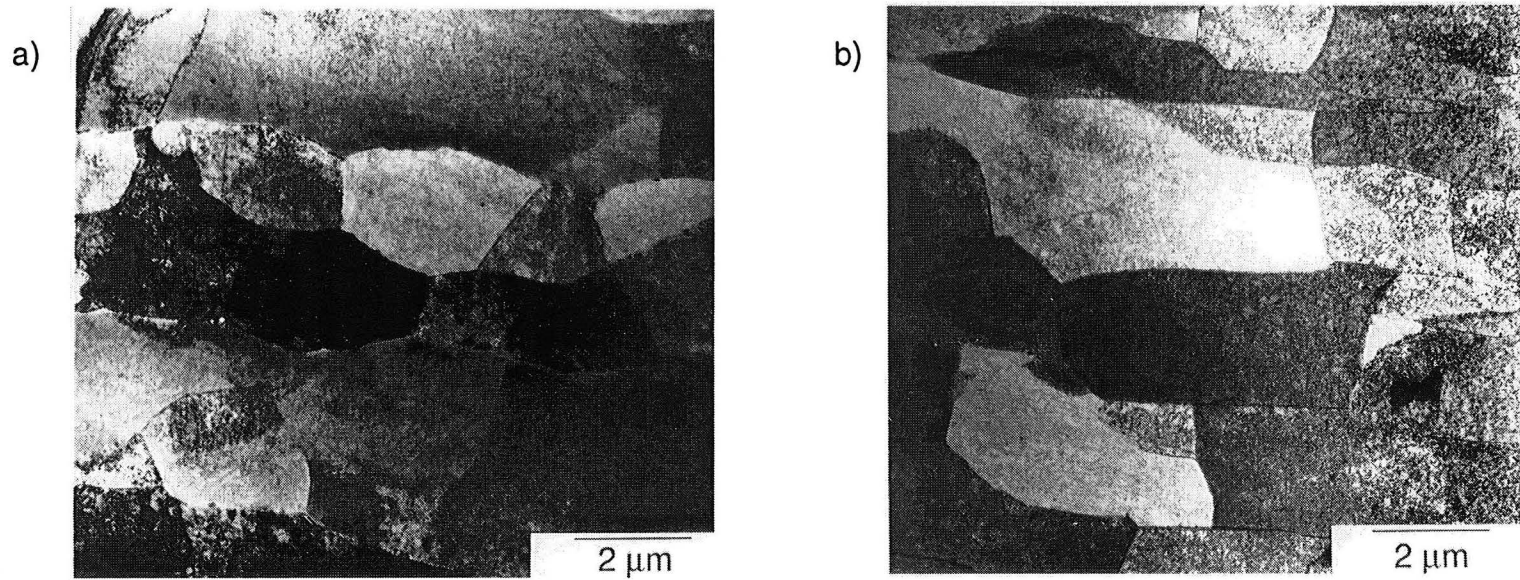
Figure 9. TEM micrographs of the AR unrecrystallized microstructure: a) several grains with subgrains distributed throughout them; b) one grain with a homogeneous distribution of subgrains.

XBB 916-4155

a)
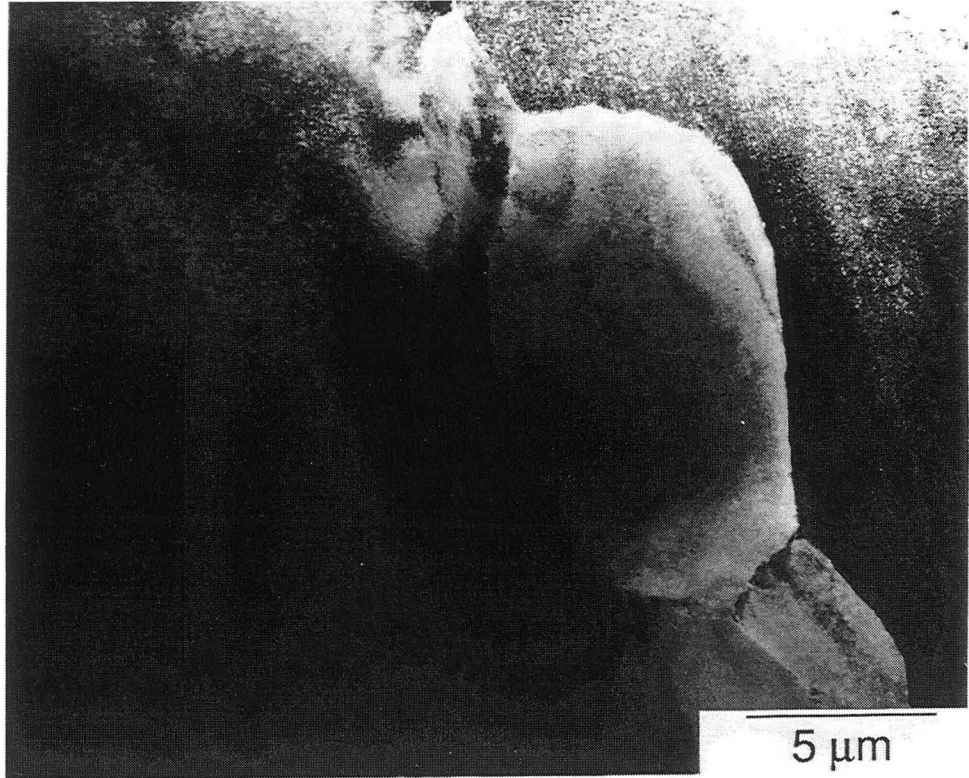
5 μm

XBB 916-4151

b)
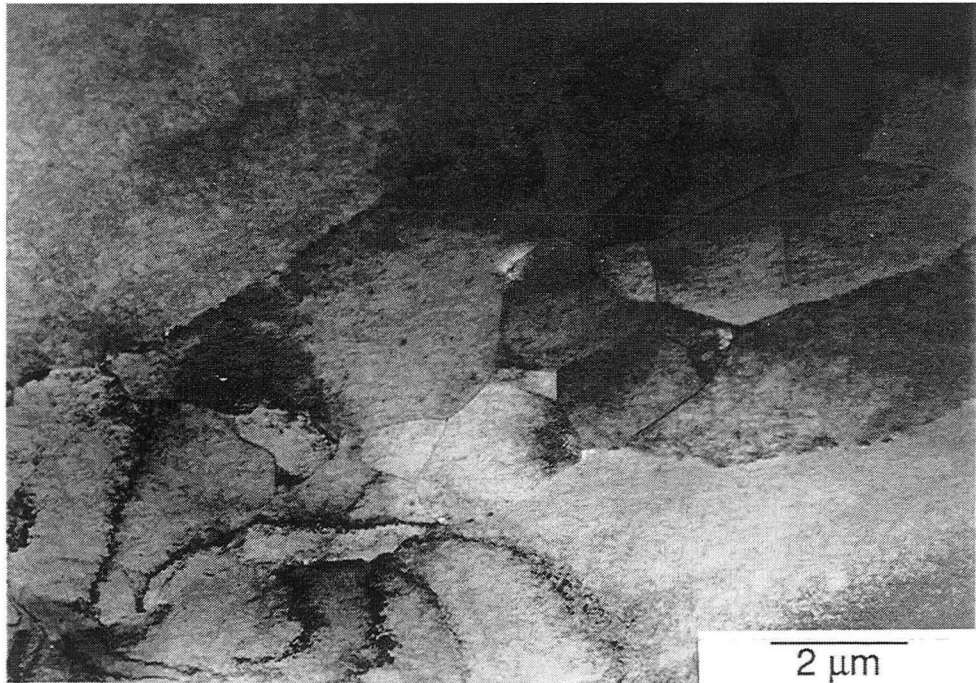
2 μm

XBB 916-4152

Figure 10. TEM micrographs of the AR recrystallized microstructure: a) several small grains reside between two very large grains and no subgrains are evident; b) some subgrain formation seen in a grain.

Figure 11. TEM micrograph of the SHT unrecrystallized microstructure. No T_1 is present.

XBB 9311-7631
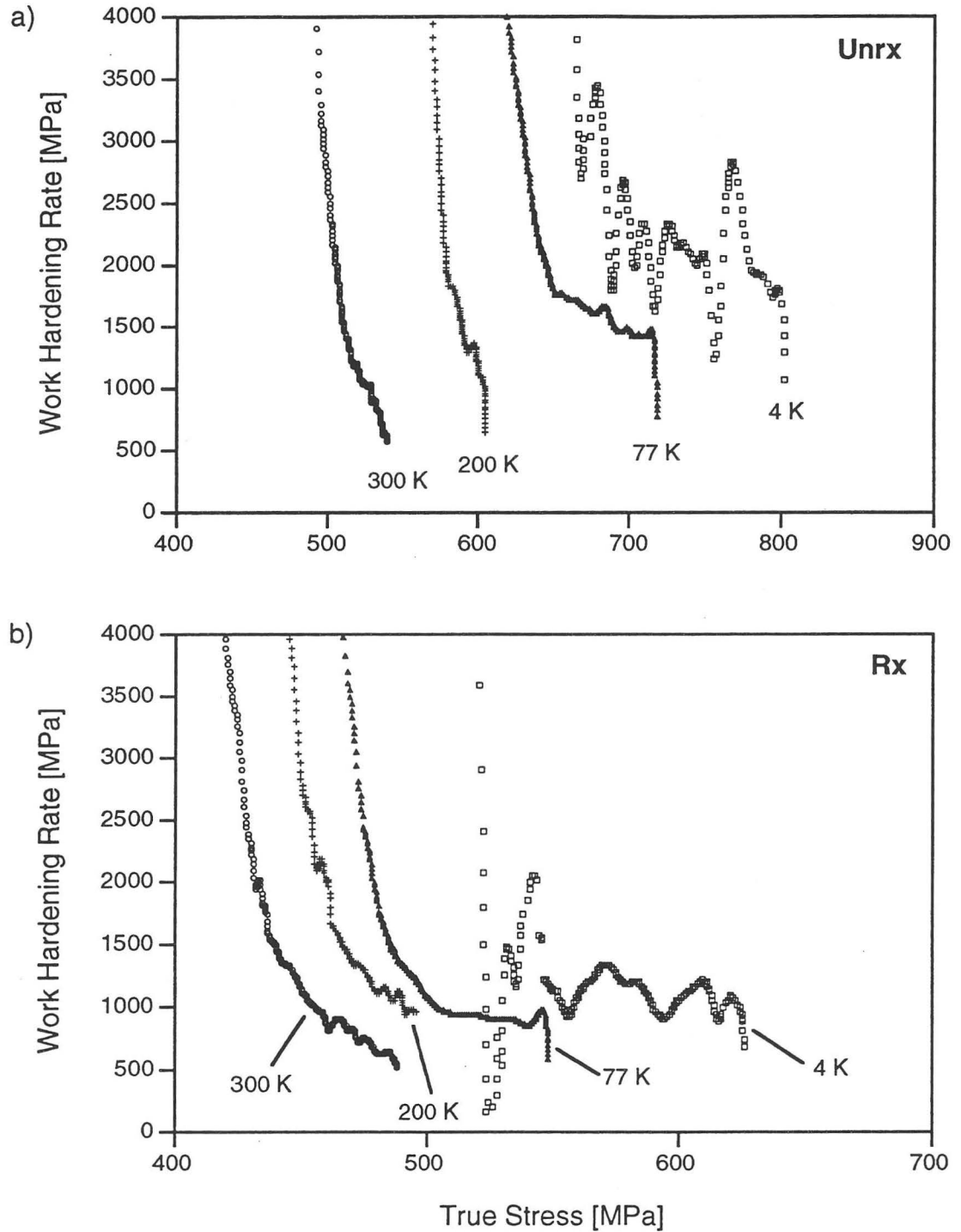
Figure 12. Work hardening curves of the AR specimens: a) unrecrystallized (Unrx) microstructure, and b) recrystallized (Rx) microstructure.

44
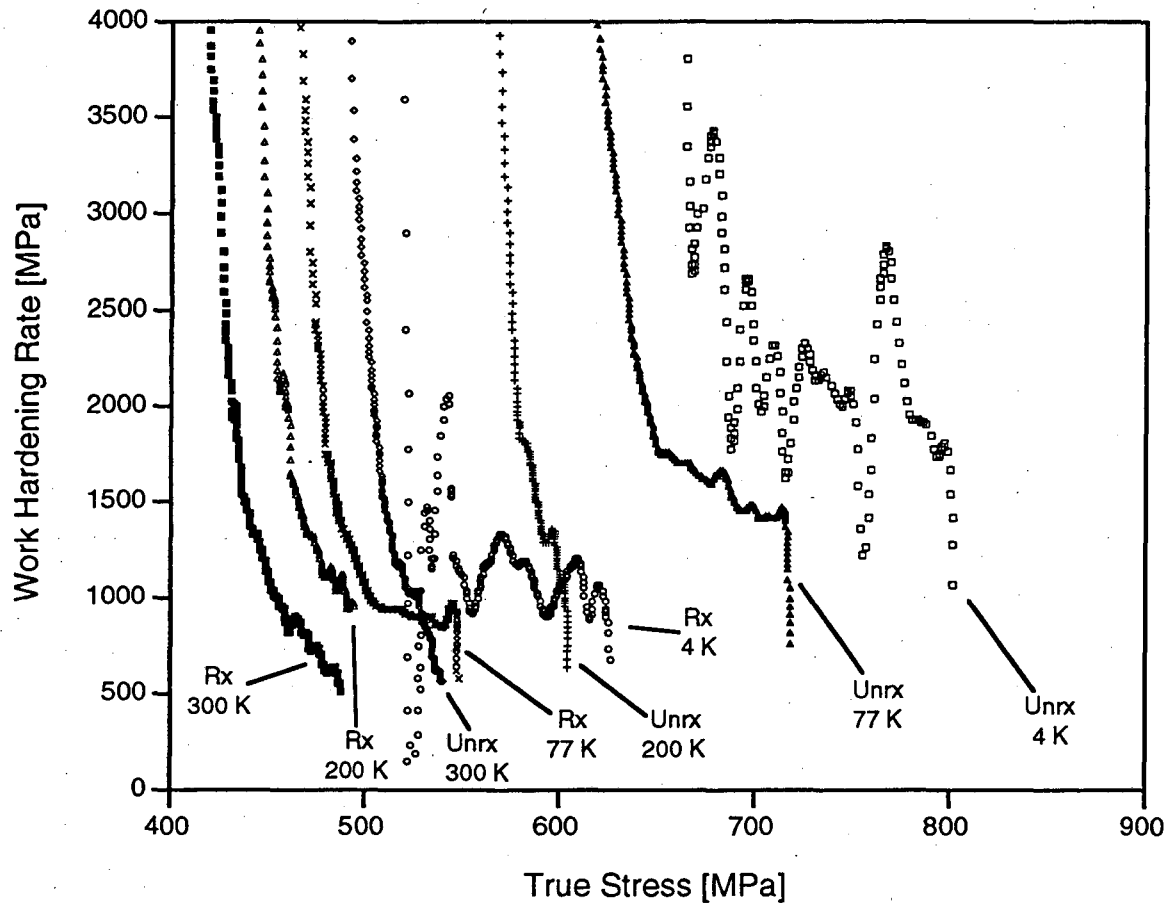
Figure 13. AR work hardening curves of both microstructures: unrecrystallized (Unrx) and recrystallized (Rx).
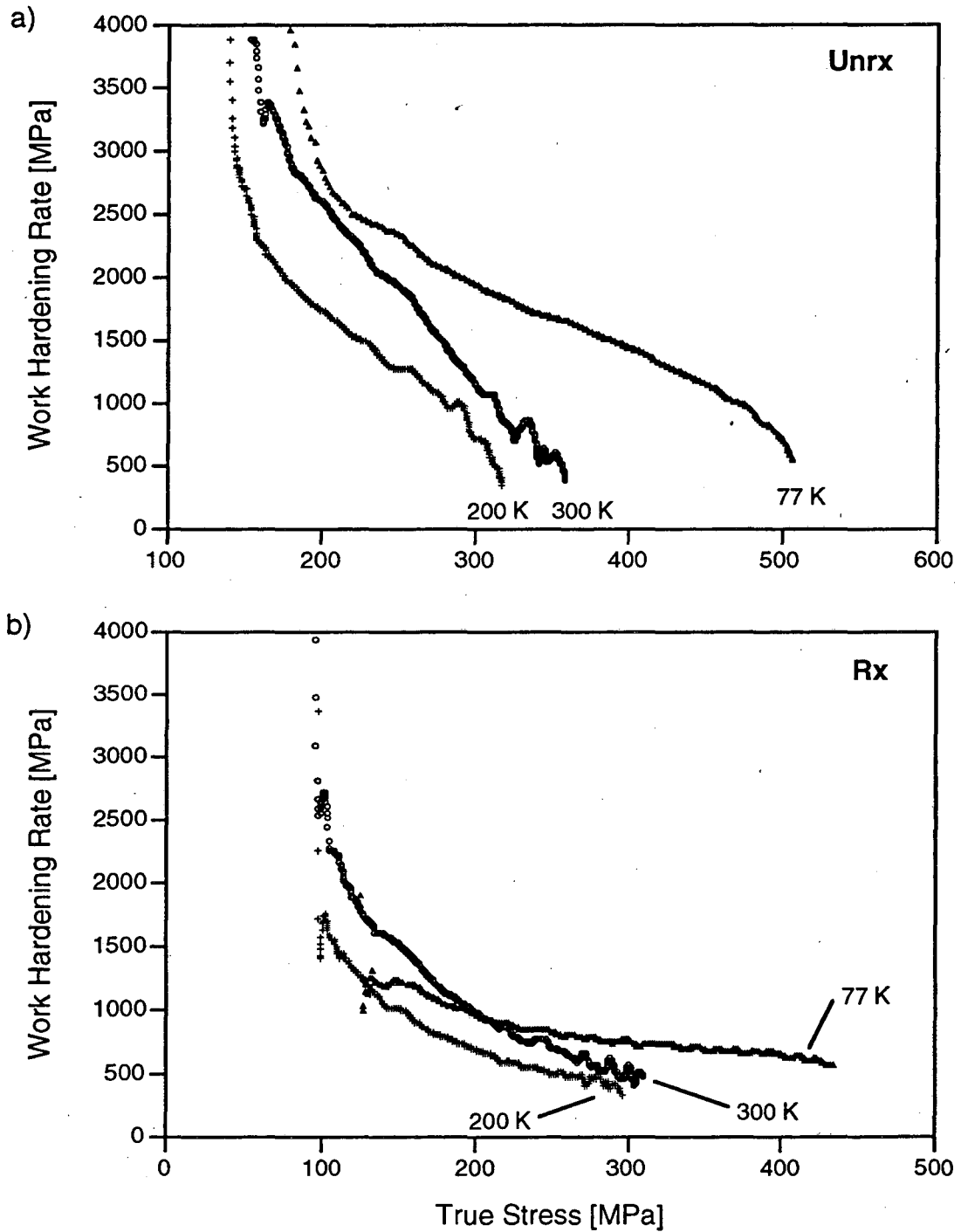
Figure 14. Work hardening curves of the SHT specimens: a) the unrecrystallized (Unrx) microstructure, and b) the recrystallized (Rx) microstructure.

46
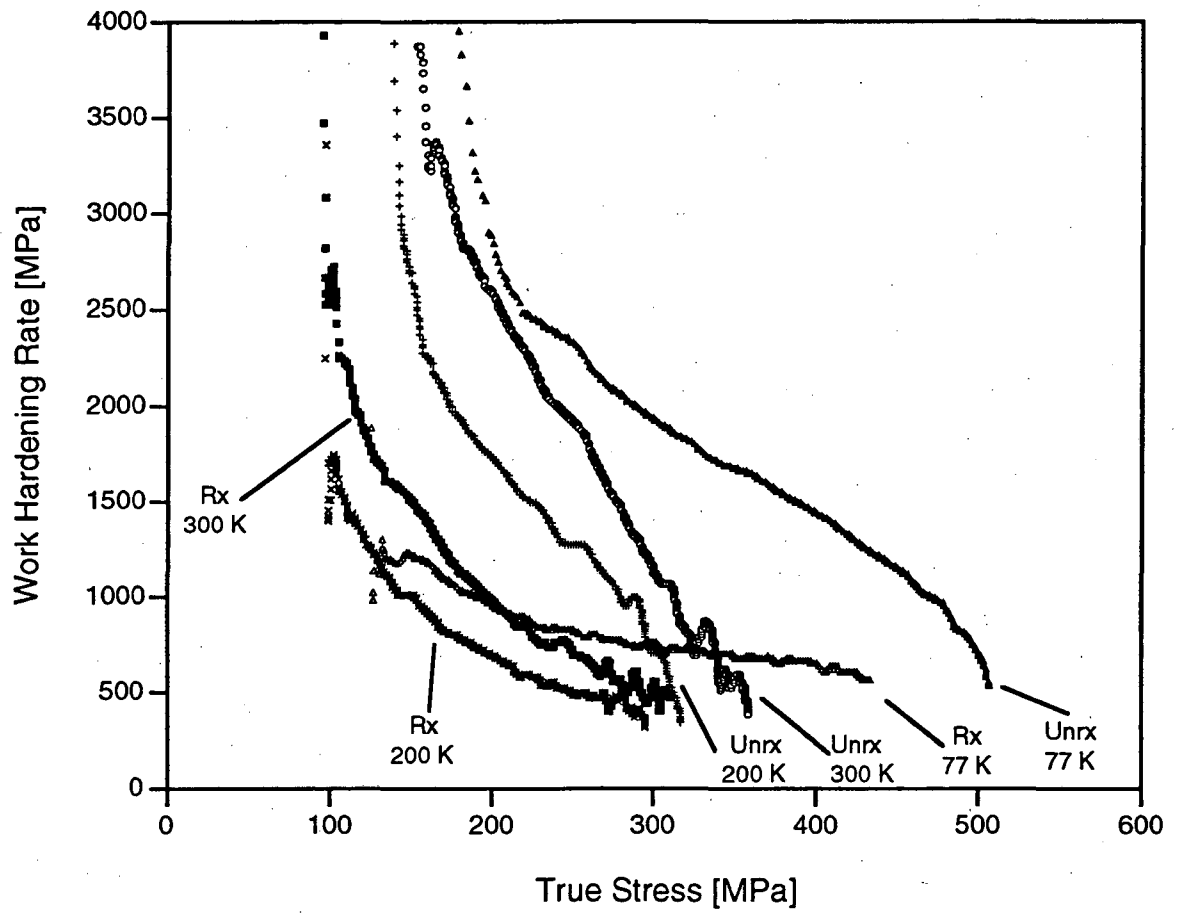
Figure 15. The SHT work hardening curves of both microstructures: unrecrystallized (Unrx) and recrystallized (Rx).

47
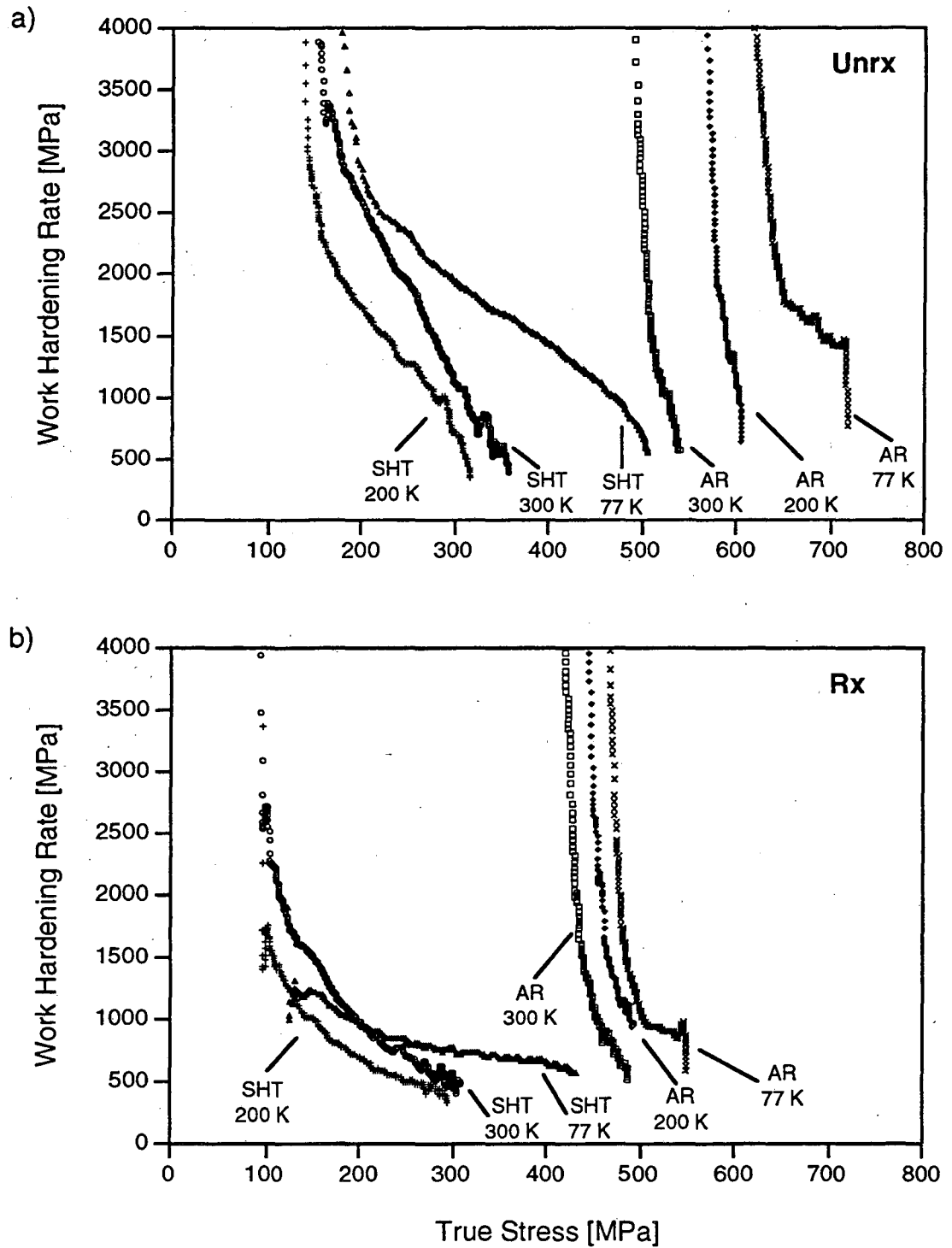
Figure 16. Work hardening plots at constant microstructure: a) both SHT and AR conditions for the unrecrystallized (Unrx) microstructure, and b) both SHT and AR conditions for the recrystallized (Rx) microstructure.
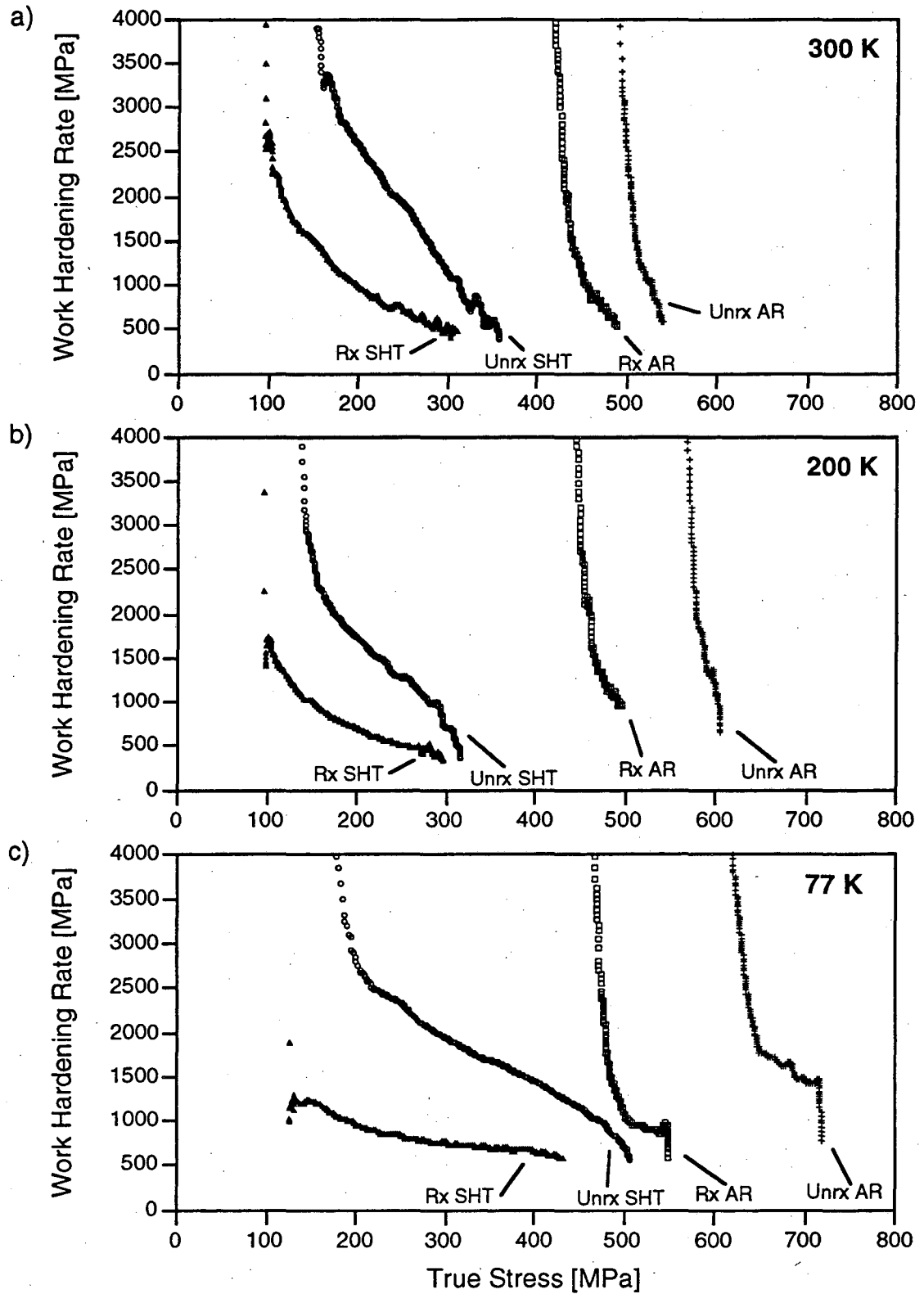
Figure 17. Work hardening curves of both microstructures and both heat treats plotted at constant temperature: a) 300 K, b) 200 K and c) 77 K.

49

Unrecrystallized Microstructure   **Recrystallized Microstructure**

300 K

77 K

200μm

σ ⟷ σ
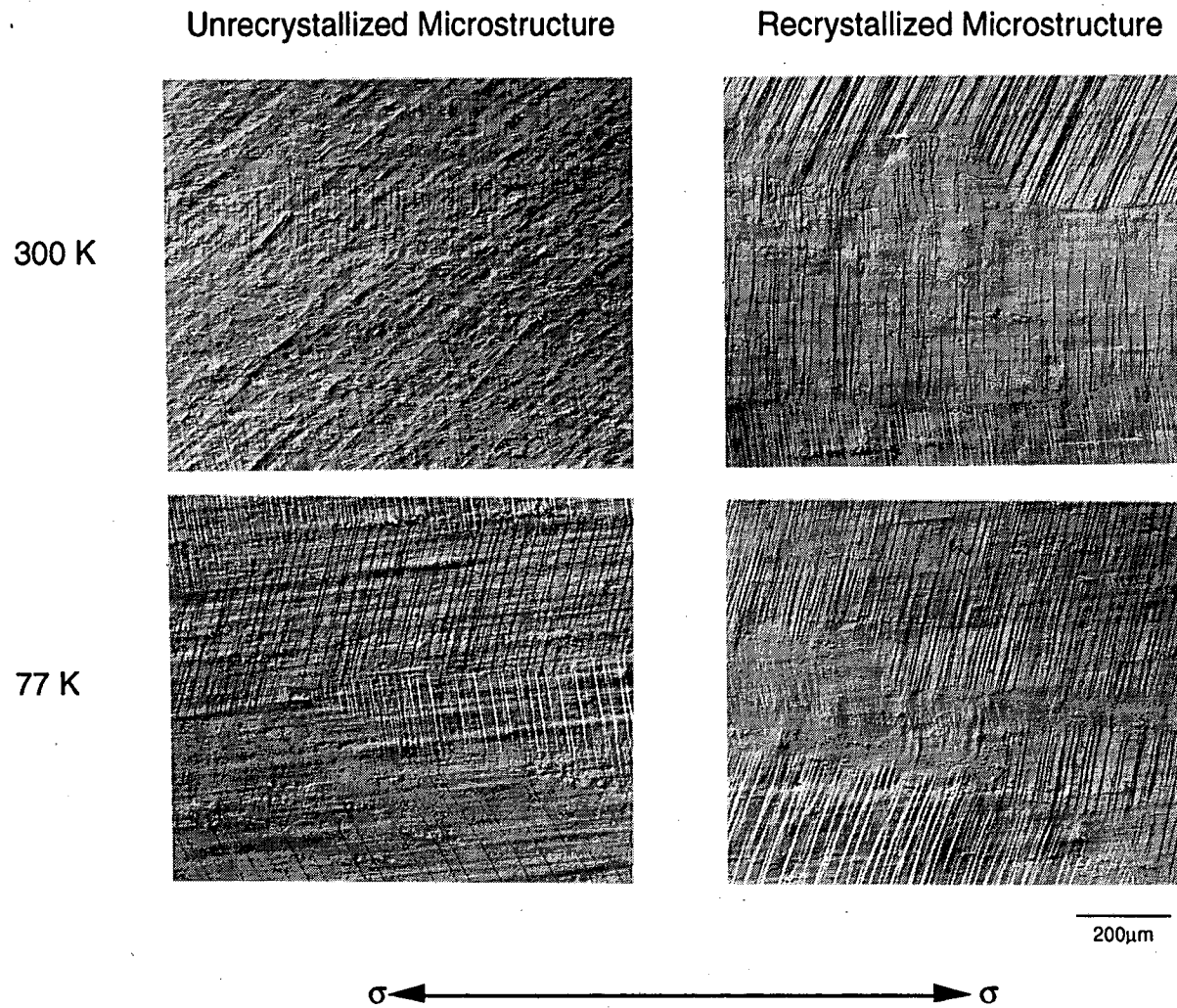
Figure 18.   Surface slip relief of specimens strained to the elastic-plastic region (ε = 0.1-0.5%).   Note the planarity of the slip.

XBB 922-1127

Unrecrystallized Microstructure

Recrystallized Microstructure

a)

b)

c)

d)

σ

σ

25 μm
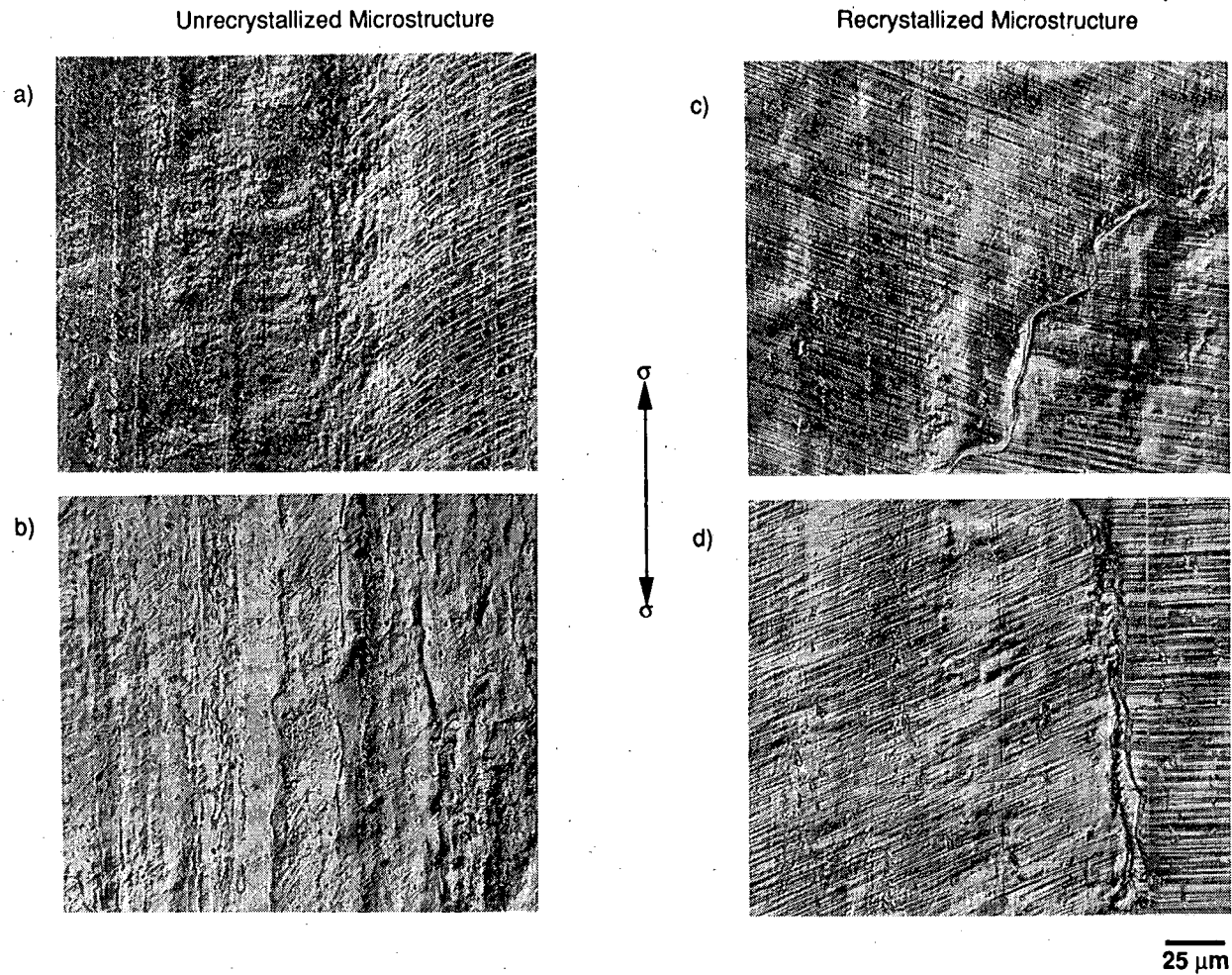
Figure 19. Surface relief of specimens strained to the fully plastic region: a) and c) were tested at 77 K, b) and d) were tested at 300 K. Specimens were strained to a) 3%; b) 2.7%; c) 3%; and d) 3.4%.

XBB 9311-7630

51
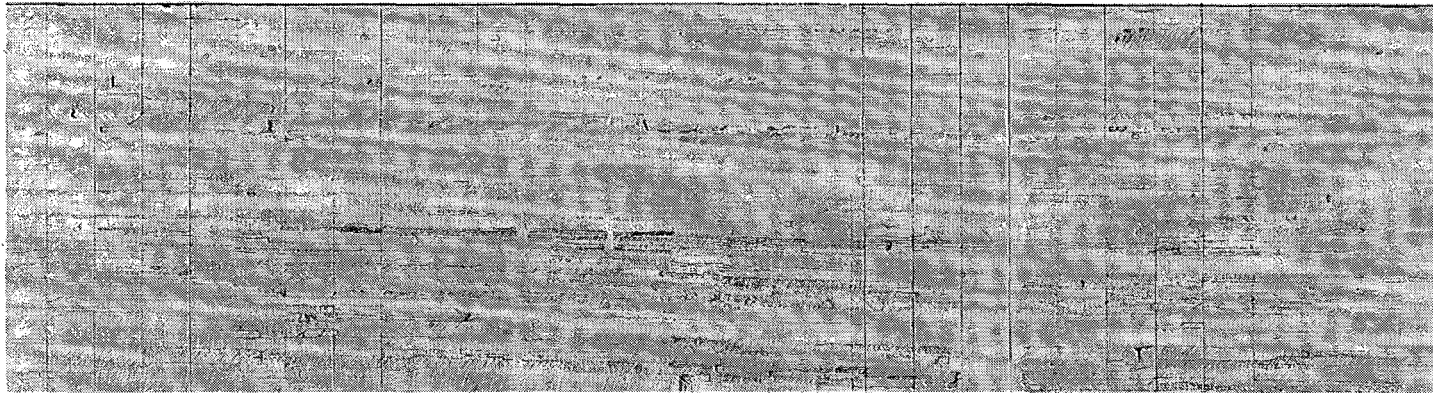
Figure 20. Sketch of the surface deformation microstructure of the unrecrystallized specimen at 77 K. The inhomogeneity in deformation is reflected by some grains showing intense slip while other grains showing very little slip (lighter in appearance). There are a few grains that do not show any deformation at all. Note that the deformation seems to occur in bands.
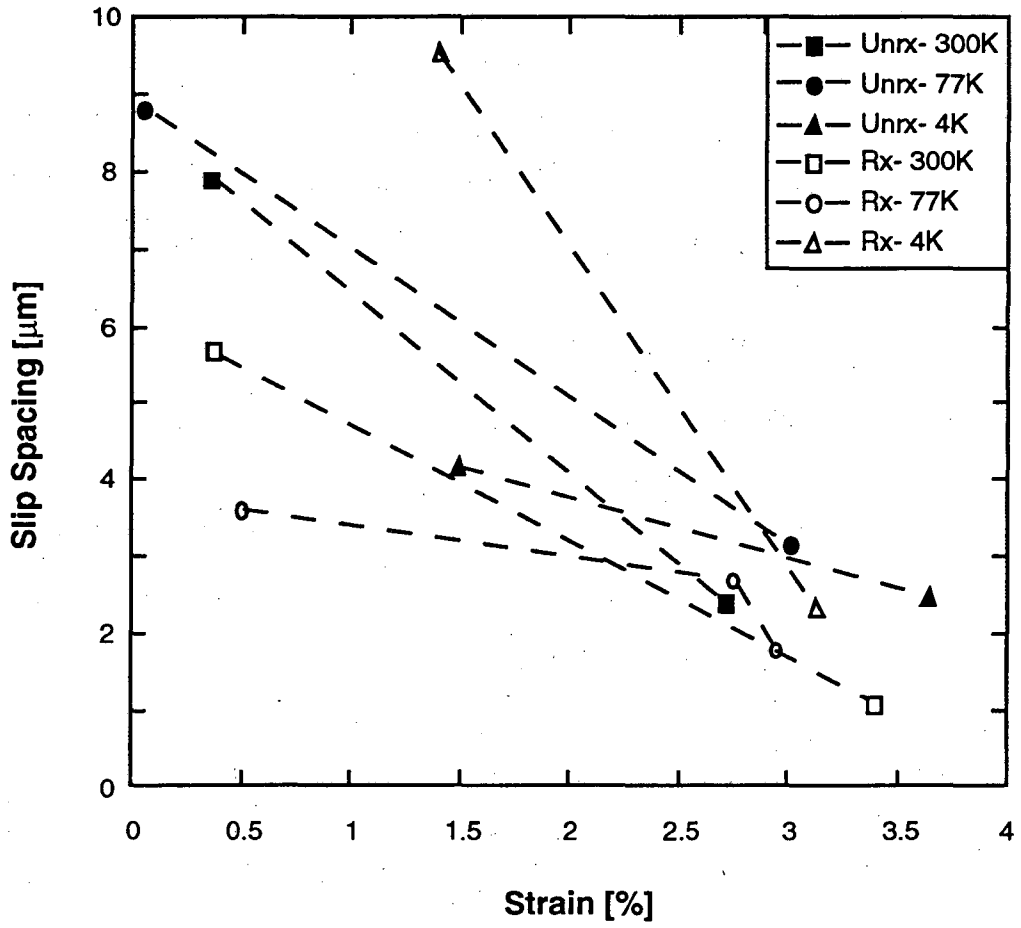
XBB 9311-7702

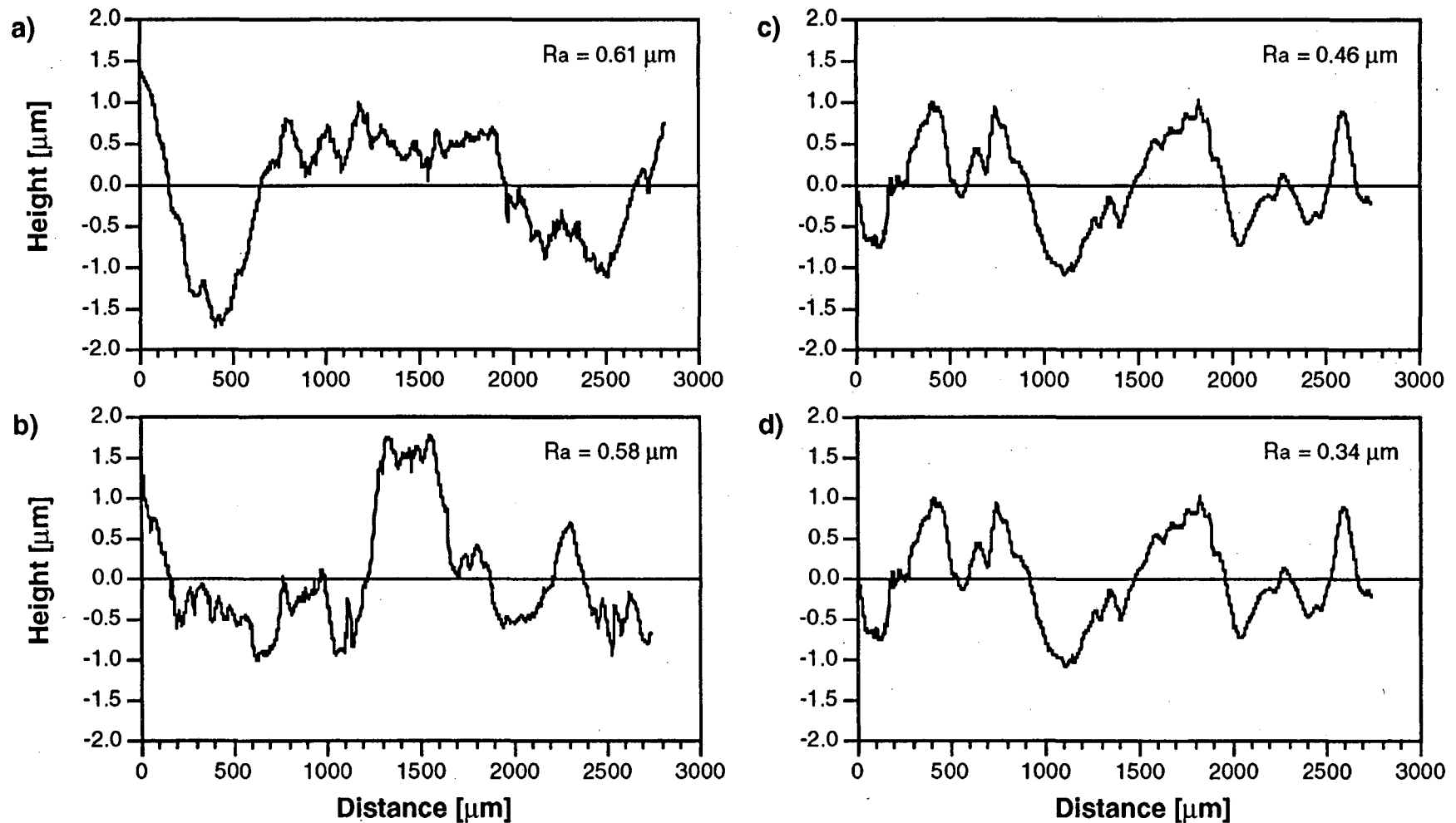Figure 21.   Plot of slip band spacing versus strain.

Figure 22. Surface profiles of AR specimens strained to ~3.1%: a) the unrecrystallized microstructure at 77 K; b) the unrecrystallized microstructure at 300 K; c) the recrystallized microstructure at 77 K; and d) the recrystallized microstructure at 300 K. Note a more dramatic increase in surface roughness for the recrystallized microstructure with decreasing temperature.
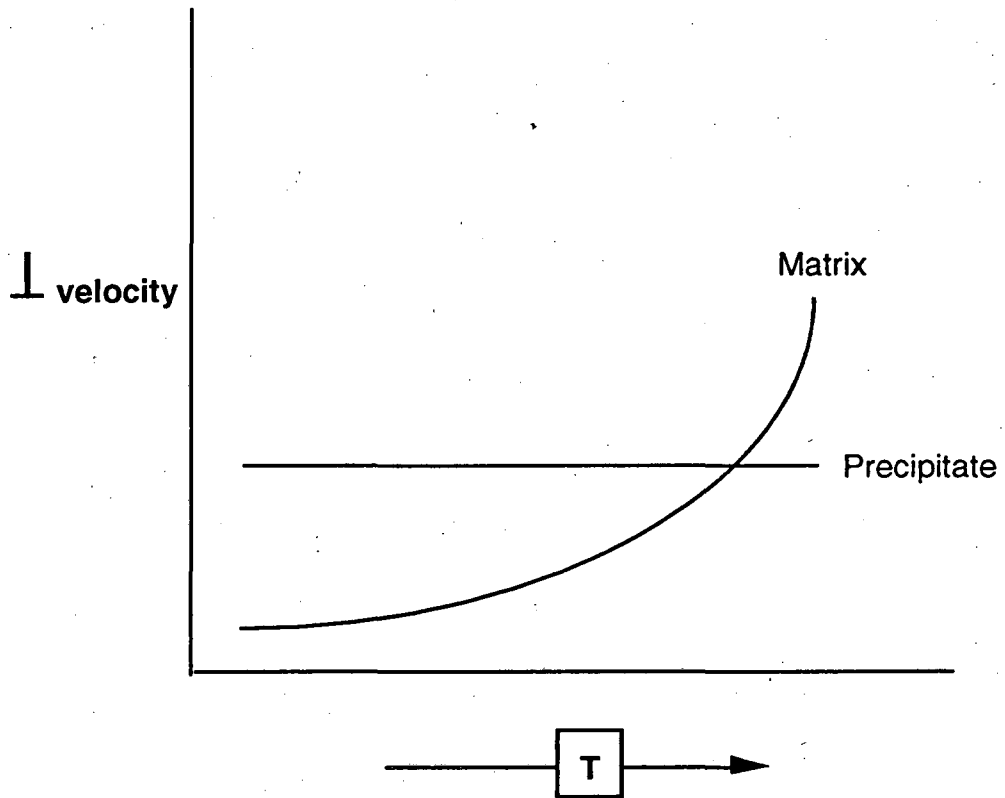
54

Figure 23. Schematic diagram of the trade-off between the matrix and precipitate contributions to dislocation velocity as the temperature increases.
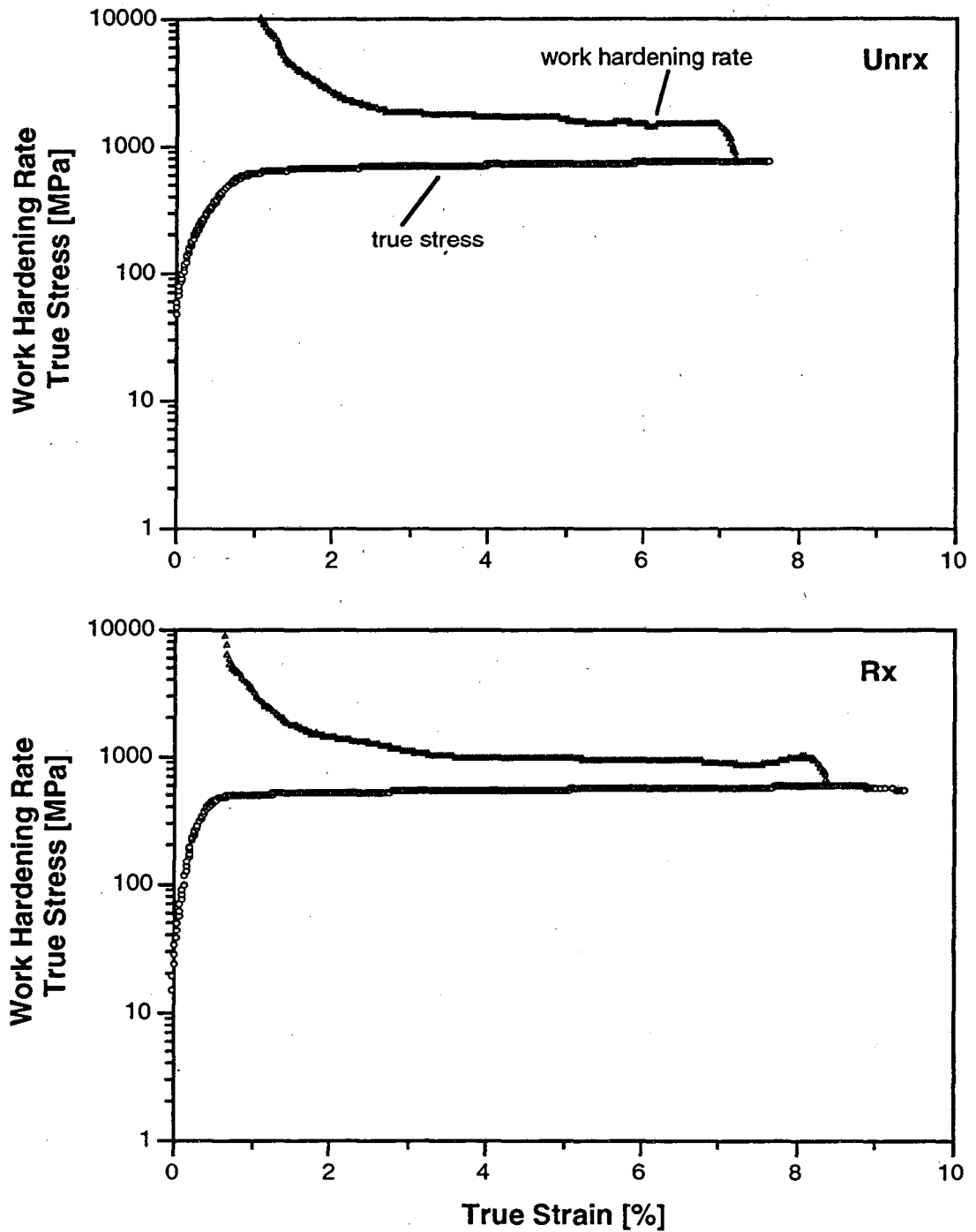
Figure 24. Plot of work hardening and true stress versus true strain for AR 77 K specimens. The drop in work hardening just before necking in figure 12 is also seen here.
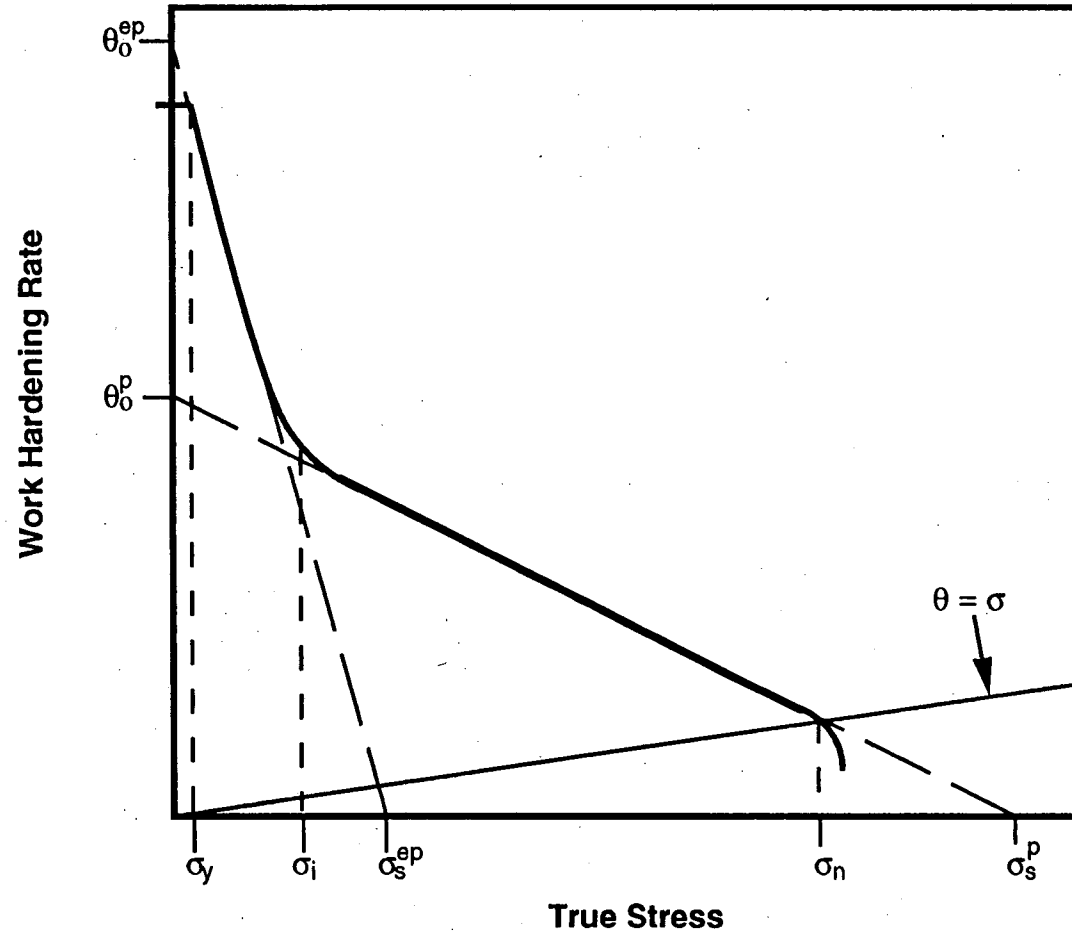
Figure 25. Schematic of the two lines fitted to the work hardening curve. The various parameters important in calculating the ideal uniform elongation are shown.